CLOUD TOP PROPERTIES AND CLOUD PHASE ALGORITHM THEORETICAL BASIS DOCUMENT

COLLECTION 006 UPDATE

W. Paul Menzel
Space Science and Engineering Center
University of Wisconsin – Madison

Richard A. Frey
Cooperative Institute for Meteorological Satellite Studies
University of Wisconsin - Madison

Bryan A. Baum
Space Science and Engineering Center
University of Wisconsin – Madison

(March 2013, version 10)

Table of Contents

1.0 Introduction

This ATBD summarizes the Collection 6 (C6) refinements in the MODIS operational cloud top properties algorithms for cloud top pressure/temperature/height and cloud thermodynamic phase. Both algorithms are based solely on infrared (IR) measurements. The C6 cloud parameters are improved primarily through: (1) improved knowledge of the spectral response functions for the MODIS 15-μm CO_2 bands gleaned from comparison of coincident MODIS and AIRS radiance measurements, and (2) continual comparison of global MODIS and measurements from the Cloud-Aerosol Lidar with Orthogonal Polarization (CALIOP) on the Cloud-Aerosol Lidar and Infrared Pathfinder Satellite Observation (CALIPSO) satellite platform. While the cloud top macrophysical parameters were provided through Collection 5 solely at 5-km spatial resolution, the cloud marcrophysical parameters are available additionally at 1-km spatial resolution in Collection 6. While both 1- and 5-km products will be available in C6, most of the improvements will be manifest in the 1-km products since the 5-km software could not be revised sufficiently to include many of the new functionality. In addition, new parameters are provided in Collection 6, including cloud top height and a flag for clouds in the upper troposphere/lower stratosphere (UT/LS), i.e., a cloud within ±2 km of the tropopause.

Mid- to high-level cloud top properties are generated using the CO_2 slicing algorithm that corrects for possible cloud semi-transparency. MODIS IR CO_2 channels are used to infer cloud-top pressure (CTP) and effective cloud emissivity (cloud fraction multiplied by cloud emissivity) at both 1-km and 5-km spatial resolution (Level 2) in Collection 6; these parameters were provided at only the 5-km resolution in previous Collections. Additionally, cloud top height (CTH) and cloud top temperature (CTT) are provided at both 1- and 5-km resolution. Note that CTH was not provided in earlier Collections. Low-level cloud top heights are derived from the 11-μm window band rather than the 15-μm CO_2 bands. However, comparison of C5 CTH with CALIOP showed significant biases in marine stratocumulus regions known to have large-scale temperature inversions. A new approach was designed and implemented to mitigate these CTH biases. Based on comparisons with CALIOP, the Collection 6 MODIS cloud top height biases for low-level boundary layer water clouds are reduced significantly from 424 m globally (although the biases are generally higher in stratocumulus regions) for Collection 5 to 197 m for Collection 6.

In earlier Collections, the IR cloud phase (henceforth IRP) determination was based solely on 8.5- and 11-μm brightness temperatures. For Collection 6, the IR phase will be provided at both 1-km and 5-km spatial resolution. The 5-km IR phase product will remain basically the same as in previous versions, except that there will now be only 3 phase categories: ice, water, and uncertain. That is, the "mixed-phase" and "undetermined" classes are combined into a single class to reduce ambiguity.

For the C6 1-km IR cloud phase product, the previous method is modified significantly to incorporate recent work involving cloud emissivity ratios, as will be discussed later in the ATBD. As with the 5-km IR phase product there will now be only 3 phase categories: ice, water, and uncertain. The approach requires a forward radiative transfer model to calculate clear-sky radiances from an input set of temperature, humidity, and ozone profiles provided by a gridded meteorological product. The IR phase results were compared to results from an updated cloud phase method available in the Version 3 CALIOP cloud products. Comparisons indicate that the new C6 MODIS IR phase algorithm improves the detection of ice clouds, with far fewer instances of optically thin ice clouds being classified incorrectly as a water cloud.

One further refinement is implemented in the 1-km products to improve the consistency between the CTH/CTP/CTT and IRP. In the description above, the CTP/CTH/CTT algorithm and the IRP algorithm are run independently of each other. When analyzing preliminary global results, an inconsistency was found: the CO_2 slicing algorithm determined that there was a high cloud, but the IRP indicated a water cloud. With the improvement in the CO_2 slicing technique afforded by the improved characterization of the spectral response functions, the sensitivity of this method improved greatly over previous Collections. To mitigate the potential lack of consistency, an IR phase result of water cloud is changed to ice cloud if the CO_2 slicing result from the 14.2-μm/13.9–μm band pair resulted in determination of a high cloud being present in a pixel. A new consistency flag is now included in the C6 1-km cloud product: IRP_CTH_Consistency_Flag_1km. This flag provides a user with the information as to whether the IR phase for a given pixel was changed to improve the consistency.

This document describes both algorithms, details the MODIS applications, and estimates the possible errors. Several references are available for further reading.

For cloud top properties, the references are:

Baum, B. A. and B. A. Wielicki, 1994: Cirrus cloud retrieval using infrared sounding data: Multilevel cloud errors. *J. Appl. Meteor*., **33**, No. 1, 107-117.

Baum, B. A., R. A. Frey, G. G. Mace, M. K. Harkey, and P. Yang, 2003: Nighttime multilayered cloud detection using MODIS and ARM data. *J. Appl. Meteor*., **42**, 905-919.

Baum, B.A. and S. Platnick, 2006: Introduction to MODIS cloud products. In Earth Science Satellite Remote Sensing, Vol. 1: Science and instruments. Edited by J. J. Qu et al., Springer-Verlag.

Baum, B. A., W. P. Menzel, R. A. Frey, D. Tobin, R. E. Holz, Ackerman, S. A., A. K. Heidinger, and P. Yang, 2012: MODIS cloud top property refinements for Collection 6. *J. Appl. Meteor. Clim.*, **51**, 1145-1163.

Chahine, M. T., 1974: Remote sounding of cloudy atmospheres. I. The single cloud layer. *J. Atmos. Sci*., **31**, 233-243.

Eyre, J. R., and W. P. Menzel, 1989: Retrieval of cloud parameters from satellite sounder data: A simulation study. *J. Appl. Meteor*., **28**, 267-275.

King M. D., W. P. Menzel, Y. J. Kaufman, D. Tanré, B. C. Gao, S. Platnick, S. A. Ackerman, L. A. Remer, R. Pincus, and P. A. Hubanks, 2003: Cloud, Aerosol and Water Vapor Properties from MODIS., *IEEE Trans. Geosci. Remote Sens.*, **41**, pp. 442-458

Menzel, W. P., W. L. Smith, and T. R. Stewart, 1983: Improved cloud motion wind vector and altitude assignment using VAS. *J. Clim. Appl. Meteor*., **22**, 377-384.

Menzel, W. P. and K. I. Strabala, 1989: Preliminary report on the demonstration of the VAS CO_2 cloud parameters (cover, height, and amount) in support of the Automated Surface Observing System (ASOS). NOAA Tech Memo NESDIS 29.

Menzel, W. P., D. P. Wylie, and K. I. Strabala, 1992: Seasonal and Diurnal Changes in Cirrus Clouds as seen in Four Years of Observations with VAS. *J. Appl. Meteor.*, **31**, 370-385.

Menzel, W. P., R. A. Frey, H. Zhang, D. P. Wylie., C. C. Moeller, R. A. Holz, B. Maddux, B. A. Baum, K. I. Strabala, and L. E. Gumley, 2008: MODIS global cloud-top pressure and amount estimation: algorithm description & results. *J. Appl. Meteor. Clim*., **47**, 1175-1198.

Naud, C. M., J. P. Muller, E. E. Clothiaux, B. A. Baum, and W. P. Menzel, 2005: Intercomparison of multiple years of MODIS, MISR, and radar cloud-top heights. Annales Geophysicae, Vol. **23** (7), 2415-2424.

Platnick. S., M. D. King, S. A. Ackerman, W. Paul Menzel, B. A. Baum, and R. A. Frey, 2003:

The MODIS cloud products: Algorithms and examples from Terra. *IEEE Trans. Geosci, Remote Sens.* **41**, 459-473.

Smith, W. L., and C. M. R. Platt, 1978: Intercomparison of radiosonde, ground based laser, and satellite deduced cloud heights. *J. Appl. Meteor.*, **17**, 1796-1802.

Wielicki, B. A., and J. A. Coakley, 1981: Cloud retrieval using infrared sounder data: Error analysis. *J. Appl. Meteor.*, **20**, 157-169.

Wylie, D. P., and W. P. Menzel, 1989: Two years of cloud cover statistics using VAS. *J. Clim.*, **2**, 380-392.

Wylie, D. P., W. P. Menzel, H. M. Woolf, and K. I. Strabala, 1994: Four Years of Global Cirrus Cloud Statistics Using HIRS. *J. Clim.*, **7**, 1972-1986.

Wylie, D. P. and W. P. Menzel, 1999: Eight years of global high cloud statistics using HIRS. Jour. Clim., **12**, 170-184.

Wylie, D. P., D. L. Jackson, W. P. Menzel, and J. J. Bates, 2005: Global Cloud Cover Trends Inferred from Two decades of HIRS Observations. *J. Clim.*, **18**, No. 15, pages 3021–3031.

For cloud phase, the references are:

Ackerman, S. A., W. L. Smith and H. E. Revercomb, 1990: The 27-28 October 1986 FIRE IFO cirrus case study: spectral properties of cirrus clouds in the 8-12 micron window. *Mon. Wea. Rev.*, **118**, 2377-2388.

Baum, B. A., P. F. Soulen, K. I. Strabala, M. D. King, S. A. Ackerman,W. P. Menzel, and P. Yang, 2000: Remote sensing of cloud properties using MODIS Airborne Simulator imagery during SUCCESS. II. Cloud thermodynamic phase. *J. Geophys. Res.*, **105**, 11,781-11,792.

Baum, B. A., W. P. Menzel, R. A. Frey, D. Tobin, R. E. Holz, Ackerman, S. A., A. K. Heidinger, and P. Yang, 2012: MODIS cloud top property refinements for Collection 6. *J. Appl. Meteor. Clim.*, **51**, 1145-1163.

Heidinger, A. K. and M. J. Pavolonis, 2009: Gazing at cirrus clouds for 25 years through a split window, part 1: Methodology. *J. Appl. Meteorol. Clim* , **48**, 2009, pp.1100-1116.

King, M. D., S. Platnick, P. Yang, G. T. Arnold, M. A. Gray, J. C. Riédi, S. A. Ackerman, and K. N. Liou, 2004: Remote sensing of liquid water and ice cloud optical thickness and effective radius in the arctic: Application of airborne multispectral MAS data. *J. Atmos. Oceanic Technol*. **21**, 857-875.

Pavolonis, M. J., 2010: Advances in extracting cloud composition information from spaceborne infrared radiances - A robust alternative to brightness temperatures, part 1: Theory. *J. Appl. Meteorol. Clim.,* **49**, 1992-2012.

Strabala, K. I., S. A. Ackerman and W. P. Menzel, 1994: Cloud properties inferred from 8-12 micron data. *J. Appl. Meteor.*, **33**, No. 2, 212-229.

Wind, G., S. Platnick, M. D. King, P. A. Hubanks, M. J. Pavolonis, A. K. Heidinger, P. Yang, and B. A. Baum, 2010: Multilayer cloud detection with the MODIS near-infrared water vapor absorption band. *J. Appl. Meteor. Clim*., 49, 2315-2333.

For AIRS – MODIS intercalibration, the references are:

Baum, B. A., W. P. Menzel, R. A. Frey, D. Tobin, R. E. Holz, Ackerman, S. A., A. K. Heidinger, and P. Yang, 2012: MODIS cloud top property refinements for Collection 6. *J. Appl. Meteor. Clim.*, **51**, 1145-1163.

Tobin, D. C., H. E. Revercomb, C. C. Moeller, and T. S. Pagano, 2006: Use of AIRS high spectral resolution infrared spectra to assess the calibration of MODIS on EOS Aqua, *J. Geophys. Res.*, **111**, D09S05, doi:10.1029/2005JD006095.

2.0 Overview

Cirrus clouds are crucially important to global radiative processes and the heat balance of the Earth; they allow solar heating while reducing infrared radiation to space. Models of climate changes will have to correctly simulate these clouds to have the proper radiative terms for the Earth's heat budget. Past estimates of the variation of cloud cover and the Earth's outgoing longwave radiation have been derived primarily from the longwave infrared window (10-12 μm) radiances observed from polar orbiting and geostationary satellites (Rossow and Lacis, 1990; Gruber and Chen, 1988). The occurrence of semi-transparent clouds is often underestimated in these single channel approaches. Recently, multispectral techniques have been used to better detect cirrus in global (Wylie et al., 2005; Wu and Susskind, 1990) and North American (Wylie and Menzel, 1989) cloud studies.

Cloud phase also plays a role in regulating the Earth's energy budget; ice and water clouds react differently to similar incident radiation. More absorption takes place in ice clouds between 10 and 12 μm than in water clouds of equal water content based on the indices of

refraction. Thus, changes in cloud phase affect climate feedback mechanisms and must be included in global climate models. In the infrared window region, changes in microphysical properties from 8 to 11 μm allow these bands to differentiate cloud phase. Past infrared single band and bi-spectral split window cloud detection techniques (Booth, 1978; Inoue, 1987; Inoue, 1989) cannot fully take advantage of these properties.

The cloud top pressure and cloud effective emissivity is determined at 5 km resolution to enable signal to noise enhancement by averaging cloudy pixels. Two inferences of cloud phase also found in the MOD06 cloud product: (1) a bispectral IR algorithm stored as a separate Science Data Set (SDS), and (2) a decision tree algorithm that includes cloud mask results as well as the IR and SWIR tests. The latter phase retrieval is stored in the MODIS "Quality_Assurance_1km" output SDS in addition to storage as an individual SDS in the Collection 5 processing stream. The decision tree algorithm provides the phase used in the subsequent optical and microphysical retrieval. The current IR phase algorithm is at 5-km spatial resolution, while the other two are at 1 km.

MODIS offers the opportunity to investigate seasonal and annual changes in the cirrus or semi-transparent global cloud cover and cloud phase with multispectral observations at high spatial resolution (one km rather than the current operational 17 km). Transmissive clouds that are partially transparent to terrestrial radiation can be separated from opaque clouds in the statistics of cloud cover (Wylie and Menzel, 1989). To date semi-transparent or cirrus clouds have been found in roughly 40% of all HIRS observations (Wylie et al., 1994).

3.0 Algorithm Description

This section presents the theoretical basis of the algorithms and practical considerations. Collection 6 will feature cloud products provided at both 1-km and 5-km resolution; the single field of view products are in support of MOD06 cloud microphysics products. The 5-km products are being provided for continuity, but the 1-km product will be the focus of Collection 6 (and future) efforts.

3.1 Theoretical Description

This section discusses the physics of deriving cloud height and amount, and cloud phase from multispectral infrared radiances from a given field of view, presents the application with MODIS data, and estimates different sources of error.

3.1.1 Physical Basis of the Cloud Top Pressure/Temperature/Height Algorithm

3.1.1.a CO_2 Slicing: Mid- to High-Level Clouds

MODIS cloud top pressure and effective cloud amount (i.e., cloud fraction multiplied by cloud emittance) are determined using radiances measured in spectral bands located within the broad 15 μm CO_2 absorption region. The CO_2 slicing technique is based on the atmosphere becoming more opaque due to CO_2 absorption as the wavelength increases from 13.3 to 15 μm, thereby causing radiances obtained from these spectral bands to be sensitive to a different layer in the atmosphere. The MODIS bands used in the cloud top pressure and amount algorithm are presented in Table 1.

Table 1: MODIS Terra spectral bands used in the cloud top pressure and amount algorithm, including bandwidths, principal absorbing components, and approximate pressure level corresponding to the peak in the individual band weighting functions.

MODIS Band Number	MODIS Bandwidth μm	Principal Absorbing Components	Approximate Peak in Weighting Function hPa
31	10.8-11.3	H_2O, CO_2	Surface
32	11.8-12.3	H_2O, CO_2	Surface
33	13.2-13.5	H_2O, CO_2, O_3	900
34	13.5-13.8	H_2O, CO_2, O_3	700
35	13.8-14.1	H_2O, CO_2, O_3	500
36	14.1-14.4	H_2O, CO_2, O_3,N_2O	300

The CO_2 slicing approach has a long history, having been applied to data from both the High resolution Infrared Radiometer Sounder (HIRS; Wylie and Menzel 1999) and the Geostationary Operational Environmental Satellite (GOES) sounder (Menzel et al. 1992; Menzel and Purdom 1994). Error analyses for the method are provided in Menzel et al. (1992) and Baum and Wielicki (1994). The historical record of cloud properties from sounder data spans more than 30 years. MODIS provides measurements at 1-km resolution and at four wavelengths located in the broad 15 μm CO_2 band. For MODIS, cloud top properties are produced for 5x5 pixel arrays wherein the radiances for the cloudy pixels are averaged to reduce radiometric noise.

Thus, the CTP is produced at 5-km spatial resolution in Collection 5. It is a goal to generate CTP at both 1- and 5-km resolution after Collection 6.

The MODIS cloud pressure is converted to cloud height and cloud temperature through the use of gridded meteorological products that provide temperature profiles at 25 hPa intervals from 1000-900 hPa, 50 hPa intervals from 900-100 hPa, and at 70, 50, 30, 20, and 10 hPa every 6 hours. The product used for this purpose is provided by the NCEP Global Forecast System (GFS; Derber et al. 1991). Differences between model-derived and measured clear-sky radiances are mitigated with a radiance bias adjustment to avoid height assignment errors. Cloud properties are derived similarly for both daytime and nighttime data as the IR method is independent of solar illumination. CO_2 slicing is most effective for the analysis of midlevel to high-level clouds, especially semi-transparent high clouds such as cirrus. One constraint to the use of the 15 μm bands is that the cloud signal (change in radiance caused by the presence of cloud) becomes comparable to instrument noise for optically thin clouds and for clouds occurring in the lowest 3 km of the atmosphere. When low clouds are present, the 11 μm data are used to infer cloud top temperature and then pressure and height via model analysis.

The CO_2 slicing technique is founded in the calculation of radiative transfer in an atmosphere with a single cloud layer. For a given cloud element in a field of view (FOV) the radiance observed, $R(\upsilon)$, in spectral band υ, can be written

$$R(\upsilon) = (1 - NE)R_{clr}(\upsilon) + NE * R_{bcd}(\upsilon, P_c) \qquad (1)$$

where $R_{clr}(\upsilon)$ is the clear sky radiance, $R_{bcd}(\upsilon, P_c)$ is the opaque cloud radiance from pressure level P_c, N is the fraction of the field of view covered with cloud, and E is the cloud emissivity. It is apparent from this expression that for a given observed radiance, if the emissivity is overestimated, then the cloud top pressure is also overestimated (putting it too low in the atmosphere).

The opaque cloud radiance can be calculated

$$R_{bcd}(\upsilon, P_c) = R_{clr}(\upsilon) - \int_{P_c}^{P_s} \tau(\upsilon, p) \frac{dB[\upsilon, T(p)]}{dp} dp \qquad (2)$$

where P_s is the surface pressure, P_c is the cloud pressure, $\tau(\upsilon, p)$ is the fractional transmittance of radiation of frequency υ emitted from the atmospheric pressure level (p) arriving at the top of the atmosphere $(p = 0)$, and $B[\upsilon, T(p)]$ is the Planck radiance of frequency υ for

temperature $T(p)$. The second term on the right represents the decrease in radiation from clear conditions introduced by the opaque cloud.

The inference of cloud top pressure for a given cloud element is derived from radiance ratios between two spectral bands following the work of Chahine (1974) and Smith and Platt (1978). The ratio of the deviations in observed radiances, $R(\upsilon)$ to their corresponding clear-sky radiances, $R_{clr}(\upsilon)$ for two spectral bands of frequency υ_1 and υ_2 viewing the same FOV is written as

$$\frac{R(\upsilon_1)-R_{clr}(\upsilon_1)}{R(\upsilon_2)-R_{clr}(\upsilon_2)}=\frac{NE_1\int_{P_s}^{P_c}\tau(\upsilon_1,p)\frac{dB[\upsilon_1,T(p)]}{dp}dp}{NE_2\int_{P_s}^{P_c}\tau(\upsilon_2,p)\frac{dB[\upsilon_2,T(p)]}{dp}dp} \tag{3}$$

For frequencies that are spaced closely in wavenumber, the assumption is made that E_1 is approximately E_2, and this allows the pressure of the cloud within the FOV to be specified. The atmospheric temperature and transmittance profiles for the two spectral bands must be known or estimated.

Once a cloud top pressure has been determined, an effective cloud amount (also referred to as effective emissivity) can be evaluated from the infrared window band data using the relation

$$NE=\frac{R(w)-R_{clr}(w)}{B[w,T(P_c)]-R_{clr}(w)} \tag{4}$$

Here N is the fractional cloud cover within the FOV, NE the effective cloud amount, w represents the window band frequency, and $B[w,T(P_c)]$ is the opaque cloud radiance. The effective cloud amount cannot be calculated without an estimate of the window band clear sky radiance. When NE is less than unity, MODIS may be observing broken cloud $(N<1,E=1)$, overcast transmissive cloud $(N=1,E<1)$, or broken transmissive cloud $(N<1,E<1)$. With an observational area of roughly five kilometer resolution, the semi-transparency for a given field of view is more often due to cloud emissivity being less than one than due to the cloud not completely covering the field of view. For most synoptic regimes, especially in the tropics and subtropics, this is found to be true (Wylie et al., 1994).

Confirmation that a cloud is upper tropospheric or lower stratospheric (UT/LS) is accomplished by determining when a measurement from a highly absorbing band, such as from a water vapor or carbon dioxide sensitive band, is warmer than a less absorbing band (Soden and Bretherton, 1993; Schmetz et al., 1997). The primary consideration is that there is a high-level temperature inversion indicated by the measurements. Radiative transfer model simulations show that when brightness temperatures increase as spectral bands become more absorbing, it is indicative of a UT/LS high cloud. For MODIS detection of UT/LS clouds, pixels are identified in which BT(13.9 μm) > BT(13.3 μm) + 0.5K. The BTD[13.9–13.3] depends on the amount of CO_2 above the cloud and the lapse rate in the stratosphere. Since CO_2 remains relatively uniform this test is seemingly more robust than and water vapor absorption channel based test such as the BTD[6.7–11].

In Collection 5, low cloud heights are determined through comparison of the measured 11–μm BT to a vertical profile of 11–μm BTs calculated from the gridded GDAS temperature, water vapor, and ozone profiles in conjunction with the PFAAST radiative transfer model. This IR window method finds a pressure/height level that matches the observation. However, this leads to biases when temperature inversions are present, with retrieved cloud heights biased high by more than 2 km with respect to collocated CALIPSO cloud products (Holz et al. 2008). Near-surface temperature inversions are common over nighttime land and in marine locations dominated by persistent stratocumulus clouds. Unfortunately, ancillary information from model output is often unreliable or at coarse spatial and vertical resolutions so one cannot reliably assume that the temperature profiles will indicate the presence of inversions.

3.1.1.b New Approach for Low-Level Clouds

For Collection 6, a different technique was developed to improve marine low cloud heights. Collocated CALIOP cloud heights, modeled and atmospherically corrected surface temperatures, and observed MODIS 11 μm brightness temperatures are combined to generate monthly zonal mean “apparent 11–μm BT lapse rates”. Since the actual boundary layer lapse rate, which may or may not include a temperature inversion, is often poorly represented in NWP profile data, the use of an apparent 11–μm BT lapse rate is an attempt to better estimate differences between the surface and measured cloud top temperatures. Low cloud heights are calculated from the difference of the clear-sky brightness temperature and the MODIS 11–μm observed cloudy

brightness temperature divided by a mean lapse rate, also called the IR window approach (IRW). It is applied when the CO_2-slicing algorithm is unable to retrieve a valid cloud top pressure (insufficient cloud signal in any of the 13.3, 13.6, 13.9, or 14.2 μm CO_2 absorption bands) and if the IRW method retrieval results in cloud-top pressures higher than 600 hPa. The IRW method will always give a result if the input radiance and atmospheric profile data are valid.

For each month of the year, three separate sets of regression coefficients were derived: one each for tropics, southern and northern latitudes (red, blue, and green lines, respectively in Figure 15). The range in latitudes appropriate for each set of coefficients was determined subjectively. In this case, the break points between the three latitude zones are at 7.8˚S and 19.5˚N latitude. Table 2 provides a list of coefficients and break points. The predicted lapse rates are restricted to a maximum and minimum of 10K km^{-1} and 2K km^{-1}, respectively.

Table 2: Fourth-order polynomial fitting coefficients and tie points for the calculation of apparent lapse rates based on 11-μm brightness temperatures as a function of latitude for each month. For each month, the top row of coefficients is for the Southern Hemisphere (SH); the middle row is for the Tropics (Trop), and the bottom row is for the Northern Hemisphere (NH). The transition from the SH to the Trop set of coefficients is given by the SH transition (latitude in degrees); likewise the transition from the Trop to the NH sets of coefficients is given by the NH transition value (latitude in degrees).

Month	Fit	a0	a1	a2	a3	a4	SH Transition (latitude)	NH Transition (latitude)
Jan	SH	2.9769801	-0.0515871	0.0027409	0.0001136	0.00000113	-3.8	22.1
	Trop	2.9426577	-0.0510674	0.0052420	0.0001097	-0.00000372		
	NH	1.9009563	0.0236905	0.0086504	-0.0002167	0.00000151		
Feb	SH	3.3483239	0.1372575	0.0133259	0.0003043	0.00000219	-21.5	12.8
	Trop	2.6499606	-0.0105152	0.0042896	0.0000720	-0.00000067		
	NH	2.4878736	-0.0076514	0.0079444	-0.0001774	0.00000115		
Mar	SH	2.4060296	0.0372002	0.0096473	0.0002334	0.00000165	-2.8	10.7
	Trop	2.3652047	0.0141129	0.0059242	-0.0000159	-0.00000266		
	NH	3.1251275	-0.1214572	0.0146488	-0.0003188	0.00000210		
Apr	SH	2.6522387	0.0325729	0.0100893	0.0002601	0.00000199	-23.4	29.4
	Trop	2.5433158	-0.0046876	0.0059325	0.0000144	-0.00000346		
	NH	13.3931707	-1.2206948	0.0560381	-0.0009874	0.00000598		
May	SH	1.9578263	-0.2112029	-0.0057944	-0.0001050	-0.00000074	-12.3	14.9
	Trop	2.4994028	-0.0364706	0.0082002	0.0000844	-0.00000769		
	NH	1.6432070	0.1151207	0.0033131	-0.0001458	0.00000129		
Jun	SH	2.7659754	-0.1186501	0.0011627	0.0000937	0.00000101	-7.0	16.8
	Trop	2.7641496	-0.0728625	0.0088878	0.0001768	-0.00001168		
	NH	-5.2366360	1.0105575	-0.0355440	0.0005188	-0.00000262		
Jul	SH	2.1106812	-0.3073666	-0.0090862	-0.0000890	0.00000004	-10.5	15.0
	Trop	3.1202043	-0.1002375	0.0064054	0.0002620	-0.00001079		
	NH	-4.7396481	0.9625734	-0.0355847	0.0005522	-0.00000300		

Aug	SH	3.0982174	-0.1629588	-0.0020384	0.0000286	0.00000060	-7.8	19.5
	Trop	3.4331195	-0.1021766	0.0010499	0.0001616	0.00000510		
	NH	-1.4424843	0.4769307	-0.0139027	0.0001759	-0.00000080		
Sep	SH	3.0760552	-0.2043463	-0.0053970	-0.0000541	-0.00000002	-8.6	17.4
	Trop	3.4539390	-0.1158262	0.0015450	0.00017117	0.00000248		
	NH	-3.7140186	0.6720954	-0.0210550	0.0002974	-0.00000150		
Oct	SH	3.6377215	-0.0857784	0.0024313	0.0001495	0.00000171	-7.0	27.0
	Trop	3.6013337	-0.0775800	0.0041940	0.0000941	-0.0000041		
	NH	8.2237401	-0.5127533	0.0205285	-0.0003016	0.00000158		
Nov	SH	3.3206165	-0.1411094	-0.0026068	0.0000058	0.00000042	-9.2	22.0
	Trop	3.1947419	-0.1045316	0.0049986	0.0001911	-0.00000506		
	NH	-0.4502047	0.2629680	-0.0018419	-0.0000369	0.00000048		
Dec	SH	3.0526633	-0.1121522	-0.0009913	0.0000180	0.00000027	-3.7	19.0
	Trop	3.1276377	-0.0707628	0.00555330	0.0001550	-0.00000571		
	NH	9.3930897	-0.8836682	0.0460453	-0.0008450	0.00000518		

3.1.2 Physical Basis of Infrared Cloud Phase Algorithm

The intent of the cloud phase discrimination method is to implement an infrared-only based technique that works independently of solar illumination conditions. Originally, Strabala et al. (1994) discussed the development and application of a trispectral IR technique that used bands at 8.5, 11, and 12 μm. This approach was simplified to a bispectral algorithm involving only the 8.5 and 11μm bands subsequent to the launch of the MODIS imagers and remained unchanged through Collection 5. Through Collection 5, the IR phase retrieval provided four categories: *ice, water, mixed phase*, and *uncertain*. A "mixed phase" cloud is thought to consist of a mixture of ice and water particles, but is ambiguous. What about a cloud that has water droplets at the top of the layer, but ice particles that grow within the cloud and fall through the cloud base? This is a relatively common situation at high latitudes. Both the 'mixed phase' and 'uncertain' categories should be considered as suspect.

With the bispectral IR method, cloud phase is inferred from the brightness temperature difference (BTD) between the 8.5 and 11 μm brightness temperatures (BTD[8.5-11]) as well as the 11 μm brightness temperature. The behavior of the IR radiances at these wavelengths for both ice and water clouds is dependent on (a) atmospheric absorption by gases such as water vapor, (b) scattering properties of ice and water clouds, which are in turn based on particle size distributions as well as particle habit distributions for ice clouds, (c) surface emissivity, and (d) cloud height. In a broad sense, absorption and emission by clouds are dependent upon the index of refraction of the cloud particles and their sizes. The absorption/emission properties are

unaffected by the particle habit (shape) or by surface roughness (e.g., Yang et al. 2013). The index of refraction (m) of the particle is given by

$$m = n_r - in_i, \tag{5}$$

where n_r is the real part and n_i, the complex portion, is an indication of absorptive properties of the material. Figure 1 depicts the real and imaginary portions of the index of refraction at wavelengths between 8 and 13 μm for both ice and liquid water. Warren (1984) provides the most recent measured data of the ice refractive index in the IR. The water refractive indices are from Downing and Williams (1975). The magnitude of n_i for ice and water are nearly equal between 8.5 and 10 μm but diverge between 10 and 13 μm. Differences in the values of the indices for water versus ice will result in distinctive reactions to similar incident radiation. To give an example: if water and ice cloud layers were to have the same temperature (i.e., exist at the same altitude), and have similar microphysical size and shape distributions, the 8.5-μm cloud radiances would be similar for both water and ice phase clouds.

As noted above, the IR thermodynamic cloud phase product through MODIS Collection 5 was based on analysis of 8.5– and 11–μm BTs in 5x5 pixel arrays where the radiances for the cloudy pixels are averaged to reduce radiometric noise. The decision tree is shown in Figure 2. This simple brightness temperature approach was used to assign each measurement to one the following classes: *ice, water, mixed-phase*, and *undetermined* (Platnick et al. 2003). Recent studies demonstrate the strengths and limitations of this product (Cho et al. 2009; Nasiri et al. 2008). Two primary limitations are that (1) optically thin cirrus may not be classified as ice phase, and (2) supercooled water or mixed-phase cloud identification is problematic when using only IR measurements.

For Collection 6, the IR phase will be provided at both 1-km and 5-km spatial resolution. The 5-km IR phase product will remain basically the same as in previous versions, except that there will now be only 3 phase categories: ice, water, and uncertain. That is, because the MODIS IR phase product has little skill in discriminating between mixed-phase and undetermined classes, these two classes are combined into an "uncertain phase" category for both the 1-km and the 5-km products in Collection 6.

The software for the 1-km retrievals is more flexible than the 5-km code, so we can refine the 1-km product much further. To mitigate the labeling of optically thin cirrus as being other than

ice phase, the methodology is enhanced by using cloud emissivity ratios as discussed in Heidinger and Pavolonis (2009); Heidinger et al. (2010); and Pavolonis (2010). The emissivity ratios are calculated as follows.

The radiance at the top of the atmosphere (TOA) can be approximated as:

$$I = (1-\varepsilon)[I_{clr} - I_{ac}] + I_{ac} + \mathrm{T}_{ac}\varepsilon B[T_{eff}] \quad (6)$$

where I is the TOA radiance, I_{clr} is the TOA clear-sky radiance, I_{ac} is the above-cloud emission contribution from the atmospheric layer, $\mathrm{T_{ac}}$ is the above-cloud transmittance, and $\mathrm{B}(T_{eff})$ indicates the blackbody radiation at the effective temperature (T_{eff}) of the cloud. From Eq. (1), the cloud emissivity for a single band is given by:

$$\varepsilon = \frac{(I-I_{clr})}{[I_{ac}+\mathrm{T}_{ac}B(T_{eff})-I_{clr}]}. \quad (7)$$

Further, the cloud emissivity for multiple bands can be related through the use of the so-called β parameter (Parol et al. 1991):

$$\beta = \frac{\ln[1-\varepsilon_y]}{\ln[1-\varepsilon_x]}, \quad (8)$$

where x and y refer to the two bands used to compute the ratio. The importance of the β parameter is that it merges measured satellite radiances with clear-sky radiances provided by either a radiative transfer model or from pixels determined to be clear sky through use of a cloud-clearing approach. By accounting for the clear-sky radiance, the influence of the surface is decreased from that found in the measured brightness temperature differences employed in the Collection 5 (and earlier) thermodynamic phase method. Figure 3 shows the logic employed for the Collection 6 1-km IR phase software. Figures 3a and 3b provides the logic over ocean and land, respectively.

We note that the IR thermodynamic phase runs separately from the cloud-top height algorithm, so that the cloud-top height is not known when computing the cloud emissivity in Eq (7). As shown in Heidinger et al. (2010), the variation of cloud emissivity with cloud height is small for cirrus clouds through the upper troposphere using IR-window bands. The reasoning for choosing the tropopause temperature is described in Pavolonis (2010) and is summarized here. An emissivity is simply a ratio of two radiance differences, and should have a value between 0 and 1. The tropopause temperature is chosen to ensure that emissivities are always less than unity. This emissivity is treated as a metric and an empirically derived threshold is placed on it. The benefit of this metric is that it accounts for clear-sky variations and in the presence of cirrus

clouds, and approximates the true cloud emissivity for high clouds. Note that this use of emissivity ratios (i.e., β) is employed primarily to improve discrimination of optically thin high-level clouds as being ice; it is not very useful to improve discrimination of water clouds.

As a complement to window bands used in the cloud emissivity method, IR absorption bands provide useful information regarding the cloud height (Heidinger et al. 2010). In the case of the IR phase, it is useful to be able to have a metric for separating low-level from high-level clouds. For MODIS, measurements are available in both the broad H_2O and CO_2 absorption regions. The 7.3 μm band is used to further discriminate between optically thin ice clouds and low-level clouds; this band is chosen instead of one of the 15-μm bands because it is less affected by detector striping. Use of the tropopause reference for the cloud emissivity calculation maintains the unique relative signatures offered by the 7.3 μm band. For lower-level clouds, the emissivities inferred from use of the tropopause pressure are significantly biased from their true value. However, the relative emissivity ratio differences remain and provide the needed skill in phase separation.

3.1.3 Mathematical Application of Cloud Top Pressure/Temperature/Height Algorithm

MODIS senses infrared radiation in seventeen spectral bands that lie between 3.75 and 14.24 μm at 1 km resolution (depending upon viewing angle) in addition to visible reflections at the same or better resolution. The four channels in the CO_2 absorption band (ch 33 at 13.34, ch 34 at 13.64, ch 35 at 13.94, and ch 36 at 14.24 μm) are used to differentiate cloud altitudes and the longwave infrared window channel (ch 31 at 11.03 μm) identifies the effective emissivity of the cloud in the MODIS field of view (FOV). Figure 4 indicates the weighting functions for the CO_2 absorption channels on MODIS.

Equation (3) will nominally be used to determine the mean cloud properties from a 5 x 5 FOV. On the left side of Equation (3), cloud radiances are determined by averaging only the radiances for those FOVs designated to be probably cloudy or cloudy by the cloud mask (at least 4 must be flagged); this enables signal to noise ratio enhancement. Clear radiances are determined in a radiative transfer calculation of the MODIS spectral band radiances using a transmittance model called Pressure layer Fast Algorithm for Atmospheric Transmittances (PFAAST) (Hannon et al. 1996); this model has 101 pressure level vertical coordinates from 0.05 to 1100 hPa. The calculations take into account the satellite zenith angle, absorption by

well-mixed gases (including nitrogen, oxygen, and carbon dioxide), water vapor (including the water vapor continuum), and ozone. The global analyses of temperature and moisture fields from the National Center of Environmental Prediction (NCEP) and Reynolds blended sea surface temperatures (Reynolds and Smith, 1994) are used to define the fields of temperature and moisture used in the forward calculation.

The right side of Equation (3) is calculated from a temperature and moisture profile and the profiles of atmospheric transmittance for the spectral bands as a function of P_c, the cloud top pressure (the integration through the atmosphere is accomplished at discrete intervals and the best pressure level rounded off to the nearest 5 hPa). Again, the NCEP global analyses of temperature and moisture fields are used. A radiance bias adjustment of measured versus calculated clear sky radiances is based on the previous eight day clear sky radiance composite; this adjustment is used to assure that the right and left sides of Equation (3) are balanced.

With the assumption that the emissivity of the clouds is the same for the two spectral bands, the P_c that best matches measured and calculated ratios is deemed a candidate solution for the cloud top pressure; the search is restricted between the surface pressure (or the top of the inversion layer) and the tropopause.

The cloud top pressure is selected with a "top-down" approach. If the most opaque bands (14.24 μm /13.94 μm) detect cloud so that $\left(R - R_{clr}\right)$ for both bands is greater than the instrument noise (conservatively estimated at 1.25, 1.00, 1.00, 0.75, 0.50 mW/m^2/ster/cm^{-1} for channels 36 – 33, 31 respectively) and Equation (3) produces a solution high in the troposphere (cloud top pressure less than 450 hPa), this is taken as the cloud top pressure solution (no other band ratios are investigated). This ratio is most sensitive to the highest clouds. If the most opaque bands do not produce a solution, a ratio of less opaque bands (13.94 μm /13.64 μm) is investigated for a solution in the upper part of the troposphere (pressure less than 550 hPa); if found this is taken as the cloud top pressure solution (no other bands are investigated). This ratio is generally more sensitive to middle-level clouds and cloud edges where information from the atmosphere below is important. If the less opaque bands do not produce a solution, a ratio of even less opaque bands (13.64 μm /13.34 μm) is investigated. This would yield the cloud top pressure for the lowest level clouds (pressure less than 650 hPa).

Thus for Aqua MODIS, ratios 36/35, 35/34, and 34/33 are used (14.24 μm / 13.94 μm, 13.94 μm / 13.64 μm, and 13.64 μm / 13.34 μm, respectively). Since Terra MODIS has severe noise problems in band 34, only ratios 36/35 and 35/33 are used.

If N_c is the number of cloudy pixels within the 5 x 5 array (estimated using the cloud mask of Ackerman et al., ATBD-MOD-35), then the representative effective cloud amount for the 5 kilometer area will be the NE determined for the cloudy pixels adjusted to represent all the pixels in the 5 x 5 array (e.g. $NE_{5x5} = N_c * NE / 25$). The cloud top temperature is taken as the brightness temperature indicated by the GFS temperature profile for level of the cloud top pressure (Menzel and Gumley, ATBD-MOD07).

If a radiance ratio cannot be calculated reliably for any of the possible band pairs because $\left(R - R_{clr}\right)$ is within the instrument noise level or none of the cloud top pressure solutions were in the appropriate range for that band pair, then a cloud top pressure is calculated directly from the infrared window band (assuming it has adequate signal to noise). The MODIS observed 11.03 μm infrared window band brightness temperature is compared with a corresponding brightness temperature profile derived from the gridded model product to infer a cloud top pressure and the cloud emissivity is assumed to be unity and $NE=N_c/25$. In this way, all clouds are assigned a cloud top pressure either by CO_2 or infrared window calculations. In the most recent collection 6, CO2 slicing solutions are avoided for known water clouds; the solution defaults to the infrared window estimate. Conversely every attempt is made to find a CO2 slicing solution for known ice clouds or mixed phase clouds. Nonetheless, very thin high clouds (likely ice clouds) are sometimes mistaken for low level opaque clouds; Wylie and Menzel (1989) found that this occurred for about half of the very thin clouds with NE less than 10%.

The data is also corrected for zenith angle to minimize the impact of the increased path length through the atmosphere of radiation upwelling to the satellite; cloud top properties are considered to be reliable for satellite viewing angles of less than 32 degrees. Table 3 demonstrates changes in cloud cover for different viewing angles.

Table 3: Aqua MODIS global cloud top pressures and effective emissivities processed at 5 km resolution for sensor scan angles less than 18, between 19 and 32, between 33 and 41, and between 42 and 55 degrees for global data on 1 Dec 2004.

%	Total	Thin	Thick	Opaque
scan angle: within 18^o (-18^o ~ $+18^o$)				
High	20.9	6.2	10.6	4.1
Middle	15.6	0.4	4.9	10.2
Low	36.0	0.0	0.0	36.0
Clear	27.5			
scan angle: $+18^o$ to $+32^o$ and -18^o to -32^o				
High	21.3	6.0	11.0	4.3
Middle	16.6	0.3	4.0	12.3
Low	36.9	0.0	0.0	36.9
Clear	25.2			
scan angle: $+32^o$ to $+41^o$ and -32^o to -41^o				
High	21.3	5.3	11.2	4.8
Middle	17.8	0.1	2.9	14.8
Low	38.2	0.0	0.0	38.2
Clear	22.7			
scan angle: $+41^o$ to $+50^o$ and -41^o to -50^o				
High	21.9	4.7	11.5	5.7
Middle	20.1	0.0	1.5	18.6
Low	39.3	0.0	0.0	39.3
Clear	18.7			
scan angle: $+50^o$ to $+55^o$ and -50^o to -55^o				
High	21.9	3.4	11.2	7.3
Middle	23.2	0.0	0.4	22.8
Low	40.4	0.0	0.0	40.4
Clear	14.4			

In summary, the calibrated and navigated MODIS data are processed for 5x5 pixel areas. Fields of view are determined to be clear or cloudy from the cloud mask (Ackerman et al. ATBD-MOD35). Where all 22 to 25 of the 1 km FOV's are clear, no cloud parameters are calculated. FOVs within satellite viewing angle of 32 degrees are considered reliable. Global coverage is realized every two days with one satellite.

(1) In Equation (3), the LHS (left hand side) is determined using the average of the measured cloudy radiances in the 5 x 5 pixel area minus a forward calculated clear radiance for the CO_2 slicing bands. The NCEP global model is used to calculate the clear radiances; these forward calculated radiances are also adjusted for radiance bias (calculated - measured clear radiance) inferred for clear FOVs from the previous eight days. The same global model is used to calculate the RHS (right hand side) for a distribution of cloud top pressures; this calculation is performed only at the grid spacing of the model.

(2) P_c derived from the most opaque bands (provided the solution is less than a designated threshold pressure) and the associated window band NE is calculated for the cloudy subset of pixels.

(3) NE for the 5 x 5 array is then determined to be $NE_{5x5} = N_c * NE / 25$

(4) If (a) cloud forcing is too small (within instrument noise), or (b) the cloud top pressure solution did not meet threshold requirements, or (c) the cloud is determined to be a water cloud, an infrared window band solution, assuming an opaque cloud, is used for the cloudy pixels and $NE_{5x5} = N_c / 25$.

The accuracy of the cloud retrieval depends on good calibration, knowledge of spectral response functions, and accurate computationally fast radiative transfer models to simulate top-of-atmosphere radiances. For the Aqua MODIS imager, the knowledge of spectral response functions (SRF) for the 13.9 μm and 14.2 μm bands has been improved through comparison with AIRS spectra. The difference between calculated and observed clear-sky radiances for the CO_2 slicing spectral bands is mitigated with a radiance bias adjustment. Finally, cloud top properties also depend on the sensor view angle. These considerations are discussed below.

As reported in Tobin et al. (2005), comparisons of co-located AIRS and MODIS observations show radiance differences in MODIS bands 33 through 36 that have significant dependency on scene temperature. They show that AIRS and MODIS radiance differences for the same scene are much smaller when the MODIS spectral response function (SRF) is shifted slightly. The temperature dependence is also greatly reduced. While the AIRS-MODIS radiance comparisons are improved through a slight shift in the SRF, no cause has been identified why such a shift could occur.

Measured and calculated clear sky radiances differ because of the cumulative effects of instrument noise, spectral response function errors, inadequate knowledge of the atmospheric

and surface state, and radiative model approximations. An adjustment is necessary to balance the right and left sides of Equation (3).

A clear sky 1^o latitudinally averaged bias adjustment is created from the 8-day clear sky bias file. The biases are composited and stored separately by day, night, land and water for the MODIS CO_2 absorption bands (bands 33-36). For example biases from 23-30 November 2004, used in processing 1 December 2004, range from -0.2 to +0.5 mW/m2/ster/μm over land and from -0.1 to +0.2 mW/m2/ster/μm over oceans. Note that land values are used for ocean ice cases in the Antarctic region. The pre-computed zonal biases are added to calculated clear-sky radiances needed for each CO_2 slicing CTP retrieval. Figure 5 shows the CTPs before and after application of the bias corrections for two 1 December 2004 granules. Note that more of the transmissive cirrus is now being reported as high cloud. Cloud heights are impacted more in the middle and high latitudes and less in the deep tropics. On this day, the amount of retrieved high-level transmissive clouds increased by 10% and 13% in the northern and southern mid-latitudes, respectively. There was an increase of 11% and 21% additional CO_2-slicing retrievals (as opposed to those from the 11 μm window) in these same regions. The radiance biases were tested globally on mid-winter, mid-summer, and transition season data; in all cases the results were more in family with other observations from lidar backscatter and HIRS CO_2 slicing.

The effect of the radiance bias adjustment is further illustrated in Figure 6 where MODIS cloud top heights are compared with backscatter data from the Cloud Physics Lidar (McGill et al., 2002) data. The radiance bias adjustment was not implemented until Collect 5; Collect 4 is largely the same algorithm except for the radiance bias considerations. Figure 6 shows that the radiance bias adjustment moves the cloud top heights (cloud top pressures converted to heights using a pressure versus geopotential height profile) from Collect 4 up about 3 km; this places Collect 5 heights within the cloud extent determined from the CPL whereas in Collect 4 they were well below the cloud bottom.

The "top-down" approach is different from earlier CO_2 slicing approaches. As described in Menzel et al. (1983), cloud top pressures were previously determined from the various ratios (14.24 μm /13.94 μm, 13.94 μm /13.64 μm, 13.94 μm /13.34 μm, 13.64 μm /13.34 μm) and the most representative cloud height and amount are those that best satisfy the radiative transfer equation for the four CO_2 bands and the infrared window. An example granule using the "top down" approach is shown in Figure 7 along with the "CO_2 radiative minimum" approach (where

valid cloud pressures and corresponding effective cloud amounts are used in an error minimization technique based on radiative transfer calculations). The top down algorithm shows fewer (presumably) spurious high clouds.

Finally, to address issues with marine stratocululus clouds in the presence of low level temperature inversions, we are using a zonal mean lapse rate (see Figure 15) and estimating the cloud top pressure from the infrared window brightness temperature, the sea surface temperature, and the lapse rate for the latitude. The cloud top height over sea level is calculated from the difference of atmosphere corrected SST minus the IRW brightness temperature divided by the lapse rate, or CTH = (atm. corr. SST - BT31) / LR.

Changes implemented for Collection 6 are

A: When using the "top-down" method with channel pairs 36/35, 35/34, 34/33 in that order to select CTP, restrict CO2 channel pair solutions to the appropriate portion of troposphere (determined by their weighting functions – 36/35 less than 450 hPa, 35/34 less than 550 hPa, and 34/33 less than 650 hPa).

B: Prohibit CO_2 slicing solutions for water clouds; use only IRW solutions. Avoid IRW solutions for ice clouds; use CO_2 slicing whenever possible.

C: Lower the "noise" thresholds (clear minus cloudy radiances required to indicate cloud presence) to 1.25, 1.00, 1.00, 0.75, 0.50 $mW/m^2/ster/cm^{-1}$ for channels 36 – 33, 31 respectively force more CO2 slicing solutions for high thin clouds.

D: Adjust ozone profile between 10 and 100 hPa to GDAS values instead of using climatology (so that CO_2 radiances influenced by O_3 profiles are calculated correctly).

E: Use Band 34, 35, 36 spectral shifts for Aqua MODIS suggested by Tobin et al. (2005).

F: Add marine stratus improvement where a constant lapse rate is assumed in low level inversions over ocean – lapse rate is adjusted according to latitude region.

G. Add UT/LS cloud flag responding to BT13.9>BT13.3+0.5.

3.1.4 Mathematical Application of the Cloud Phase Algorithm

Figure 3 is a flow chart of the refined IR thermodynamic phase method over ocean (Figure 3a) and land (Figure 3b). Three different band pairs are used: 7.3 μm/11 μm, 8.5 μm/11 μm, and 11 μm/12 μm. The 8.5 μm/11 μm band pair is primarily sensitive to ice phase clouds, while the information content in the 11 μm/12 μm band pair is related to cloud opacity. The 7.3 μm/11 μm

pair helps to separate high from low clouds. The following example demonstrates how the use of these band pairs improves the identification of optically thin ice clouds.

Figure 8 shows global results for daytime IRP at a grid resolution of 0.2˚. Figure 8a (upper panel) shows the Collection 5 phase results, and Figure 8b shows results from application of the new method. For the Collection 5 results, pixels that are not positively identified as either *ice* or *water* are now labeled as *uncertain*. Note that pixels that are classified as "uncertain" in Figure 8a are now classified more often as containing ice clouds in Figure 8b. There is still no attempt to classify cloud pixels as perhaps having a lower-level water cloud layer underneath the ice layer. Phase discrimination for supercooled water clouds remains problematic.

A Collection 6 IR thermodynamic phase product will be provided at both 1-km and 5-km resolution, and at both spatial resolutions the "mixed-phase" category is being eliminated as a separate category so that results will be provided as *ice*, *water*, or *uncertain*. However, the improved cloud phase product described above will be provided only at 1-km resolution. The 5-km phase product will continue to be provided for continuity, but the 1-km product is the focus of Collection 6 (and future) efforts.

3.1.5 Estimate of Errors Associated with the Cloud Top Properties Algorithm

In the study of Wylie and Menzel (1989), the CO_2 cloud heights derived from VAS (VISSR Atmospheric Sounder) data over North America were found to be of good quality when compared to three other independent sources of cloud height information. Results showed: (a) for about thirty different clouds, the CO_2 heights were within 40 hPa rms of cloud heights inferred from radiosonde moisture profiles; (b) in 100 comparisons with lidar scans of clouds, the CO_2 heights were 70 hPa lower on the average and were within 80 hPa rms; (c) satellite stereo parallax measurements in 100 clouds compared to within 40 hPa rms. The CO_2 heights appeared to be consistent with other measurements within 50 hPa and the effective fractional cloud cover within 0.20 in most cloud types. The CO_2 slicing technique works best for middle and high clouds, but has trouble with very low clouds.

3.1.5.a Errors Associated with the Assumption of Constant Emissivity

To minimize differences in the cloud emissivity between the two spectral channels, the CO_2 slicing method is applied to channels that are spectrally close in wavenumber. These are generally adjacent channels with a narrowband sensor. Zhang and Menzel (2002) showed that

cloud emissivity ratio adjustments of 5% for adjacent CO_2 channels have a small effect on cloud properties derived with the CO_2 slicing method. For optically thin clouds, a cloud emissivity ratio increase of 10% (longer wavelengths divided by shorter wavelengths) increased the CTP by 35 hPa and ECA by 1%.

3.1.5.b Errors Associated with the Assumption of a Thin Cloud Layer

The CO_2 slicing algorithm assumes that all of the radiative effects of the cloud occur in the top thin layer. This makes the mathematics tractable. If the radiative transfer integral of Equation (3) were to include a cloud term where the cloud has finite depth, then knowledge of the vertical structure of the cloud would be required. There are an infinite variety of combinations of cloud depths and vertical combinations that could produce the same integrated radiative signature; a unique solution is not possible. Any initial assumption of cloud structure biases the cloud top and bottom solution derived in the radiative transfer formulation.

The thin layer cloud approximation is investigated in Smith and Platt (1978). They found that errors in the height assignment approaching one-half (one-quarter) the thickness of the cloud were introduced for optically thin (thick) clouds where the integrated emissivity is less than (greater than) .6. The largest errors will be associated with physically thick but optically thin cirrus clouds. For optically thin (very transparent) cirrus with 100 hPa depth the error in the height estimate is roughly 50 hPa.

Wielicki and Coakley (1981) also discussed the consequences of the thin layer cloud approximation. They concluded that the algorithm solution (P_c) would be near the center of the cloud for optically thin clouds and near the top of the cloud for optically thick clouds. This is similar to a center of mass concept. The algorithm solution will thus be close to the "radiative center" of the cloud. Thus, P_c is somewhere between the cloud top and its center varying with the density of the cloud.

Cirrus height errors are also discussed in Wylie and Menzel (1989) where VAS cloud top pressure estimates were compared to cloud tops measured by lidars and by the stereo parallax observed from the images of two satellites at two different viewing angles. VAS CO_2 channels (14.25, 14.01, and 13.33 μm) are similar to three of the four on MODIS. In the lidar comparison, the VAS inferred cloud top pressure over an observation area was compared to the highest lidar observation in the same area; these clouds had to be radiatively thin for the lidars to see through

the cloud tops. Definition of a single cloud top was often difficult within a cloud layer; the lidar heights varied considerably (by more than 50 hPa) from one cloud element to another in the same cloud layer. On the average, the VAS P_c was found to be 70 hPa larger (lower cloud altitude) than the tops seen on the lidars. The CO_2 slicing technique was sensing the mean height; the VAS heights were comparable to the lidar top heights to within half the cloud thickness. In the comparisons to stereo parallax measurements for thin transmissive clouds, the VAS heights showed little bias. It was often difficult to measure parallax for thin transmissive clouds, as they appeared fuzzy with poorly defined boundaries in the images. Since the image of the clouds is more indicative of the center of the diffuse cloud mass than its outer boundaries, the parallax method is also sensitive to the radiative center of mass rather than the physical tops of these clouds. Thus, in these intercomparisons of actual measurements, the CO_2 cloud top pressures were found to be within the accuracy suggested by theoretical considerations.

3.1.5.c Errors Associated with the Presence of a Lower Cloud Layer

The algorithm assumes that there is only one cloud layer. However, for over 50% of satellite reports of upper tropospheric opaque cloud, the ground observer indicates additional cloud layers below (Menzel and Strabala, 1989). To understand the effects of lower cloud layers, consider the radiation sensed in a cloudy field of view. For a semi-transparent or cirrus cloud layer, the radiation reaching the satellite, R, is given by

$$R = R_a + E * R_c + (1 - E) * R_b \qquad (10)$$

where R_a is the radiation coming from above the cloud, R_c is the radiation coming from the cloud itself, R_b is the radiation coming from below the cloud, and E is the cloud emissivity. When a lower cloud layer is present under the semi-transparent or cirrus cloud, R_b is smaller (i.e., some of the warmer surface is obscured by the colder cloud). If prime indicates a two layer cloud situation of high semi-transparent cloud over lower cloud, and no prime indicates a single layer high semi-transparent cloud, then

$$R_b' < R_b, \qquad (11)$$

which implies

$$R' < R. \qquad (12)$$

Thus the difference of cloud and clear radiance is greater for the two layer situation,

$$\left[R_{clr} - R'\right] > \left[R_{clr} - R\right] \tag{13}$$

The effect of two cloud layers is greater for the 13.3 micron channel than for the other CO_2 micron channels, because the 13.3 micron channel "sees" lower into the atmosphere (Figure 4 shows the weighting functions where the 13.3 peaks lower in the atmosphere than the other CO_2 channels). So using the 13.9/13.3 ratio as an example

$$\left[R_{clr}(13.3) - R'(13.3)\right] > \left[R_{clr}(13.9) - R'(13.9)\right] \tag{14}$$

This reduces the ratio of the clear minus cloud radiance deviation in Equation (3) because the denominator is affected more than the numerator (when the less transmissive channel is in the numerator),

$$\frac{\left[R_{clr}(13.9) - R'(13.9)\right]}{\left[R_{clr}(13.3) - R'(13.3)\right]} < \frac{\left[R_{clr}(13.9) - R(13.9)\right]}{\left[R_{clr}(13.3) - R(13.3)\right]}, \tag{15}$$

or Left' < Left, where Left refers to the left side of Equation (3). An example plot of P_c versus Right (where Right refers to the right side of Equation (3)), shown in Figure 9, indicates that Left' < Left implies $P_c' > P_c$. Thus, when calculating a cloud pressure for the upper semi-transparent cloud layer in a two cloud layer situation, the CO_2 slicing algorithm places the upper cloud layer too low in the atmosphere.

An example from 25 October 1990 using VISSR Atmospheric Sounder (VAS) data is presented to illustrate further the magnitude of the errors that can be induced by lower level clouds (results for other days and other situations were found to be comparable). Ground observers in Omaha, Nebraska reported thin cirrus clouds with no other underlying clouds present. The ratio of the 13.9 to 13.3 micron satellite observed radiance differences between clear and cloudy FOVs (the left side of Equation (3)) is 0.36 on 25 October. This implies single layer cloud at 300 hPa (solving the right side of Equation (3) for P_c as shown in Figure 9).

R' has been modeled for a semi-transparent cloud at 300 hPa with an underlying opaque cloud layer at 920, 780, 670, 500, and 400 hPa (each configuration produces a different ratio in the left side of Equation (3), Left'). The different Left' suggest different P_c' solutions as Left' is matched to Right, the right side of Equation (3). In the absence of any knowledge of a lower layer, the CO_2 algorithm integrates the right side of Equation (3) from the surface to an incorrect P_c'. Figure 9 shows Right as a function of P_c for the situation of 25 October. The errors in

calculated cloud top pressure from the original 300 hPa solution, $P_c' - P_c$, are shown as a function of height of the underlying opaque cloud layer in Figure 10a for 25 October.

In the two cloud layer situation, the position of the lower cloud layer affects the accuracy of the estimate of the height of the upper cloud layer. Opaque clouds in the lower troposphere underneath high cirrus have little affect on the cirrus P_c. Inspection of the spectral transmittance show that neither the 14.2 or the 13.9 micron channels are very sensitive to radiation from low in the troposphere, while the 13.3 micron channel senses only about half of the radiation from below 800 hPa. Opaque clouds in the middle troposphere, between 400 and 800 hPa, underneath high cirrus, cause the cirrus P_c to be overestimated (lower in the atmosphere) by up to 220 hPa (this extreme occurs for the very thin high cirrus cloud with NE of 0.10). The decreases in R_b produce smaller ratios for the left side of Equation (3) which in turn produces larger estimates of P_c. Opaque clouds high in the atmosphere, underneath higher cirrus, have little effect on the cirrus P_c, since the height of the lower opaque layer approaches the height of the semi-transparent upper cloud layer and the CO_2 algorithm is going to estimate a height in between the two layers.

The errors in P_c were also examined for different emissivities of transmissive clouds (see Figure 10b). This was modeled by varying the emissivity and forming new ratios on the left side of Equation (3). The maximum cloud top pressure error of roughly 220 hPa occurred in very thin cloud with emissivity of 0.10. The error in P_c reduced as the emissivity of the transmissive clouds increased. For a cloud with emissivity of 0.5, the maximum error in P_c is about 100 hPa. For more dense clouds with emissivity of 0.9, the maximum error in P_c is less than 20 hPa. The VAS data have shown a nearly uniform population of emissivity center around 0.5 (Wylie and Menzel, 1989), so one can conclude that the errors in the cloud top pressure caused by underlying clouds should average under 100 hPa.

Multi-layer cloud situations (transmissive over opaque cloud) cause the height estimate of the upper cloud to be about 100 hPa too low in the atmosphere on the average. The error in transmissive cloud height is largest when the underlying opaque layer is in the middle troposphere (400- 700 hPa) and small to negligible when the opaque layer is near the surface or close to the transmissive layer. The error in effective emissivity increases as the opaque layer approaches the transmissive layer; when they are coincident, the effective emissivity is assumed

to be one. In summary the cloud forcing from two layers is greater than the cloud forcing from one layer; assuming only one cloud layer when two exist causes the CO_2 solution to put the cloud between the two layers with larger effective emissivity. This suggests that, overall, global cloud parameter estimates will be a little low in the atmosphere and with an effective emissivity a little too high.

Recent work has suggested that the radiative transfer equation in a two layer cloud situation can be solved from the CO_2 radiance observations. The two layer cloud forcing can be written, where u is the upper cloud layer and l is the lower cloud layer,

$$R - R_{clr} = N_l E_l \left[1 - N_u E_u\right] \int_{P_s}^{P_{cl}} \tau dB + N_u E_u \int_{P_s}^{P_{cu}} \tau dB \qquad (16)$$

Thus the two layer cloud forcing is characterized by four unknowns $N_l E_l$, $N_u E_u$, P_{cl}, and P_{cu}. Using the measured cloud forcing in the CO_2 channels, a solution for upper and lower cloud pressures and effective cloud amounts is calculated. The algorithm selects spectrally close pairs of CO_2 channels. For each pair of cloud forcing measurements, all possible $N_l E_l$, $N_u E_u$ are calculated as a function of P_{cl}, P_{cu}. From this array of possible solutions, the selected solution best satisfies the radiative transfer equation for all spectral channels. Since four unknowns offer more degrees of freedom than two unknowns, the two layer solution is preferred over the one layer solution. Indication of when to use the two layer solution is sought through inspection of 4.0 μm versus 11.0 μm radiance scatter plots for the 5 x 5 pixel area (when radiances for the two spectral channels lie on two or more straight lines then the presence of two or more cloud layers is suggested). More development work remains, before the two layer solution can be incorporated into the cloud parameter algorithm.

3.1.5.d Errors from an Inaccurate Estimate of the Surface Temperature

Zhang and Menzel (2002) note that surface emissivity was found to have a small effect on the cloud properties for thin cirrus and no effect on them for thick clouds. For thin clouds, CTP increased by about 15 hPa when the surface emissivity was decreased by 2%, and the associated increase in ECA was approximately 1%.

The CO_2 slicing algorithm has little sensitivity to surface temperature. The weighting functions for the CO_2 channels indicate that very little radiation from the Earth surface is detected by the satellite radiometer in these spectral bands (14.2 and 13.9 μm observations don't

even see the ground). Table 4 indicates the changes in cloud top pressure associated with changes in estimates of surface temperature inferred from a recalculation of the right side of Equation (3); the atmospheric profile of 25 October was used as an example (other situations yield similar results). When the surface temperature T_{sfc} is assumed to be 5 C too warm, the cloud top pressure P_c is 32 hPa smaller (higher in the atmosphere); when T_{sfc} is assumed to be 5 C too cold, P_c is 26 hPa larger (lower in the atmosphere). In other words, when the surface temperature guess doesn't track surface warming (cooling), then the cloud layer is calculated to be too low (high).

Table 4. The changes in cloud top pressures (P_c) and effective emissivities determined from the CO_2 slicing algorithm after changes to the estimated temperature profile and surface temperature (using the data of 25 October 1990).

	Guess Error (guess - truth)		Cloud Top Pressure and Effective Emissivity Error with additional errors from faulty cloud screening for contaminating clouds at					
					300hPa		700hPa	
met cond	sfc DTs	atm $DT_{(p)}$	DP_c	$D(NE)$	DP_c	$D(NE)$	DP_c	$D(NE)$
a	+5 K	0 K	-32 hPa	-.09				
b	-5	0	+26	+.13	+39 hPa	+.13	+20 hPa	+.09
d	0	+2	+10	+.03				
c	0	-2	-13	-.03				
ad	+5	+2	-20	-.07				
ac	+5	-2	-44	-.11				
bd	-5	+2	+37	+.19	+50	+.19	+31	+.14
bc	-5	2	+16	+.09	+28	+.09	+09	+.06

Possible meteorological conditions that could cause indicated errors in the guess
a indicates nocturnal cooling
b indicates solar heating
c indicates warm frontal passage
d indicates cold frontal passage

Table 4 also indicates an additional effect that arises when the surface temperature is assumed to be too cold. In the cloud screening process, some cloudy FOVs are inferred to be

clear and R_{clr} is reduced for all spectral channels. Thus the left side of Equation (3) is reduced (when the less transmissive channel is in the numerator) and P_c goes even larger (lower in the atmosphere). The last four columns of Table 4 show the total error when 25% of the FOVs are incorrectly inferred to be clear for a guess that is 5 C too cold; when high clouds at 300 hPa contaminate the clear radiance determination, P_c is 39 hPa larger (representing an additional error of 13 hPa), and when low clouds at 700 hPa contaminate the clear radiance determination, P_c is 20 hPa larger (representing an offsetting error of 6 hPa).

The surface temperatures are monitored hourly with the SVCA conventional observations; errors of 5 C are unusual, but do occur in the western mountains where surface observations are too sparse to accurately represent the varying altitude conditions. We conclude that nominal diurnal changes in surface temperature will not affect the CO_2 slicing solutions of P_c by more than 50 hPa.

Furthermore, fictitious reports of transmissive clouds cannot be produced by changes in the ground surface temperature, since two of the three channels do not see the ground. As witnessed in Table 4, effective emissivity estimates are relatively insensitive to surface temperature excursions of 5 C; NE changes of about 0.10 are found.

The preceding discussion also implies that the CO_2 algorithm is insensitive to surface emissivity changes since 5% changes in surface temperature can be equated with roughly 7% changes in surface emissivity for the long wavelength channels.

3.1.5.e Errors from an Inaccurate Estimate of the Temperature Profile

Table 4 also shows the changes in cloud top pressure associated with changes in estimates of temperature profile as well as surface temperature for the example of 25 October. When the entire temperature profile was changed by +/- 2 K in the calculation of the right side of Equation (3), the resulting changes were very small - about 10 hPa for P_c and 0.03 for NE. These errors are roughly inversely proportional to the lapse rate at the altitude of the cloud. When the surface temperature and the atmospheric temperature were adjusted by 5 and 2 K respectively, maximum errors of roughly 40 hPa in P_c and 0.20 in NE were found for the situation where the surface temperature was underestimated and the atmospheric temperature was overestimated (perhaps possible in nearly clear sky with strong solar heating producing a very large lapse rate in the lower atmosphere). Where the surface temperature and the

atmospheric temperature were both underestimated (possible in a warm frontal passage), the cloud was estimated to be too low in the atmosphere by 20 hPa in P_c and too opaque by 0.10 in NE.

Experiments were also conducted simulating errors localized to only one level of the temperature profile. The results (not shown) were modified minimally. Little sensitivity is apparent for temperature errors low in the atmosphere ($P_c > 700$), as expected from inspecting the transmittances of the MODIS CO_2 channels. An error of 2 C for a level between 700 and 300 hPa can produce a shift of up to 30 hPa in the cloud top pressure. This should be viewed in conjunction with the lapse rate of 5 C per 50 hPa for the example of 25 October. Here and in other situations inspected, the errors in the CO_2 slicing cloud top pressure estimate, DP_c, caused by sounding errors, DT, in layers where the CO_2 spectral channels have sensitivity, are found to be roughly inversely proportional to the lapse rate at the level of the cloud, L; this can be expressed as $DP_C = DT / L$.

3.1.5.f Errors Associated with Instrument Noise

The VAS radiometer is accurate to better than 1 mW/m2/ster/cm^{-1}. This corresponds to less than 1 K in the CO_2 channels for temperatures ranging from 220 to 320 K. Noise affects the ability of the VAS to detect thin cirrus. Noise of 1 K implies that effective cloud emissivities of less than 10% cannot be resolved for high clouds (using $D(NE) = DR / (R - R_{clr})$. In our earlier work of 1989, it was found that about half of the very thin clouds with NE less than 0.10 were classified incorrectly as low opaque cloud observations (this represented about 5% of all observations); it was also found that about half of these very thin clouds were correctly classified by the CO_2 slicing algorithm.

The CO_2 slicing technique cannot measure the properties of clouds where the contrast of radiation from cloud free and cloud obscured observations is too small for reliable discrimination in satellite CO_2 spectral radiances (when radiance differences are less than .5 mW/m^2/ster/cm^{-1} cloud properties are not calculated). This occurs for very thin cirrus (as discussed in the previous paragraph) and for some low clouds below 700 hPa. Clouds below 700 hPa were assumed to have an effective emissivity of one, thus preventing the interpretation of low broken cloud as cirrus. Occasionally, low clouds were also reported in situations of clear sky with tropospheric

temperature inversions; this created problems in early morning statistics during the winter months.

When noise is introduced in one channel of the CO_2 radiance ratio, the left side of Equation (3) changes. Using the example of 25 October once again, Figure 9 shows the noise induced changes in the ratio. The extremes produce a P_c that is 50 hPa lower or make it impossible to have a solution in the atmosphere. This example is representative of several noise investigations using the CO_2 slicing algorithm; sensor noise typically has an effect of less than 50 hPa.

3.1.5.g Conclusions of the Cloud Top Pressure and Emissivity Error Studies

(i) Errors associated with the assumption of constant emissivity for the CO_2 channels are negligible.

(ii) The CO_2 slicing algorithm determines the height of the radiative center of the cloud; for optically thick clouds this is near the cloud top while for optically thin clouds it is near the cloud middle.

(iii) Multi-layer cloud situations where an opaque cloud underlies a transmissive cloud cause errors in the height of the transmissive cloud of about 100 hPa for most cases (the cloud is determined to be too low in the atmosphere). The error in transmissive cloud height is largest when the underlying opaque layer is in the middle troposphere (400- 700 hPa) and small to negligible when the opaque layer is near the surface or close to the transmissive layer.

(iv) When the surface temperature guess doesn't track surface warming (cooling), then the cloud layer is calculated to be too low (high). Nominal diurnal changes in the ground temperature are typically tracked to better than 5 C in the CO_2 slicing algorithm, so that they have little effect on the ability to detect transmissive clouds or to determine their heights.

(v) The CO_2 solution is largely insensitive to errors in the temperature sounding in the lower troposphere. There are often compensating effects in the integration of the atmospheric column. The errors in the CO_2 slicing cloud top pressure estimate caused by sounding errors in layers where the CO_2 spectral channels have sensitivity are roughly inversely proportional to the lapse rate at the level of the cloud.

(vi) Instrument noise causes the CO_2 slicing algorithm to miss roughly half of the thin cirrus with effective emissivity less than 0.10; this represents about 5% of all observations.

3.1.6 Error Estimates of Cloud Phase Algorithm

Modeled results and observations of the infrared cloud phase determination suggest it is very reliable in the determination of warm low-level water clouds and high-level ice clouds with optical thicknesses above approximately 0.5. The most difficulty pertains to (a) midlevel clouds for which unambiguous cloud phase discrimination is problematic, (b) extremely optically thin cirrus, and (c) when thin cirrus overlies a lower-level cloud (i.e., multilayered clouds). Verification of cloud phase is being made through comparison with the CALIPSO/CALIOP Version 3 cloud phase product. Known sources of error are discussed below.

3.1.6.a Errors Due to Mixed Phase Cloud Scenes

Single-layered clouds of wide spatial extent having cloud-top temperatures in the range between 250K and 270K are prevalent in the storm tracks in both the Northern and Southern Hemispheres. Unambiguous phase discrimination for these clouds is extremely difficult. Current efforts are to improve cloud phase discrimination for clouds at temperatures between 233K and 273K, the range over which the presence of supercooled water is possible.

3.1.6.b Errors Due to Non-uniform Surface Emissivities

The current version of the bispectral technique assumes a uniform surface emissivity for both IR bands. This is certainly not the case for many different ground surface types, including bare soils and deserts. Gao and Wiscombe 1994 modeled the effects of different surface types on the BTD[8 – 11] values based on laboratory surface emissivity measurements. Their results suggest that certain types of bare rock, and dry vegetation lead to misidentification of cloud phase by the tri-spectral technique due the resultant location of the brightness temperatures differences on the scatter diagram. Many different MODIS and MAS data sets over numerous surface types have been investigated to date.

3.1.6.c Errors Due to Instrument Noise

An investigation into the effects of MAS pixel averaging on brightness temperature differencing was conducted, with distinct cloud signals becoming apparent after averaging over a 5 x 5 pixel box. This lowers the NEDT values for the 8, 11 and 12 micron channels (as evaluated for MAS 5 December 1993 data) to 0.13, 0.09 and 0.15 K respectively. The MODIS

NEDT specifications of these infrared bands at 300 K is 0.05 K, suggesting that the noise is within the limits for cloud phase delineation.

3.2 Practical Considerations

3.2.1.a Radiance Biases and Numerical Considerations of Cloud Top Pressure Algorithm

The MODIS measured radiances have biases with respect to the forward calculated radiances using model estimates of the temperature and moisture profile for a given field of view. There are several possible causes for this bias: these include calibration errors, spectral response uncertainty, undetected cloud in the FOV, and model uncertainty. Solution of Equation (3) and (4) uses measured and calculated cloud forcing (clear minus cloudy FOV radiances) and thus requires that this bias be minimized. Techniques developed at the European Centre for Medium range Weather Forecast to characterize the HIRS radiance bias with respect to the ECMWF model (Eyre, 1992) are being employed in the MODIS cloud algorithm. In order to reduce systematic biases from being introduced into the cloud height calculations, simulated MODIS spectral radiances from clear-sky FOVs are compared to the corresponding observed radiances for several days at the beginning of each month processed. A regression relationship is developed for a correction to the simulated radiances during subsequent reprocessing of the data. One relationship is derived for ocean regions; another for land suirface. (This is done automatically, with the radiances stored in a rotating file containing data from several previous days.)

The measured and the calculated radiance gradient ratios in Equation (3) do not always converge within the allowable pressure bounds (between the tropopause and the top of the inversion layer or the surface). Solutions are not accepted if found at the boundaries, even though there may be a good meteorological reason to accept these values. In these cases the opaque cloud solution from the window channel is used.

Evaluation of the integrals in the right side of Equation (3) or (3') are performed at 50 hPa increments (the integration through the atmosphere is accomplished at discrete 50 hPa intervals and the best pressure level interpolated to 10 hPa). When the slope in Figure 9 increases, instrument noise causes more error in the cloud top pressure determination. It has

been found that mid-latitudes have greater slopes than the topics, thus cloud top pressures in the tropics might be slightly less error prone.

3.2.1.b Numerical Considerations of Cloud Phase Algorithm

The implementation of the cloud phase algorithm is very straightforward, and requires that the cloud mask product (MOD35) be available as well as the 8.5 and 11-μm BT's for each cloudy pixel.

3.2.2 Programming Considerations of Cloud Top Properties Algorithm

Processing is accomplished for every 5 x 5 pixel area (5 km resolution at nadir). The clear sky radiances come from a spatial analyses of the pixels designated clear by the cloud mask. Spatial registration of the channels must occur, so that FOVs can be collocated with ancillary data.

The CO_2 slicing algorithm has been used for the past nine years on VAS data over North America and for the past seven years on global HIRS data. It is a robust algorithm. The census of cirrus clouds derived from both of these efforts has been published in refereed literature.

Processing time for the MOD06CT algorithm are derived from using the direct broadcast version on a Sun solarix x86 machine. To processs 5000 lines (~10 minutes) requires ~ 15 minutes.

The product Level 2 MOD06CT-5km volume per granule (5 minutes of data) is 14 MB. A full day of MODIS processing results in a volume load of 14 MB/granule * 288 granules/day = 4.0 GB/day for the parameters listed in Table 9. It should be noted that product MOD06 also includes particle radius and and optical thickness retrievals at 1km during the daytime. This increase the size of daytime granules to 60 MB.

3.2.3 Validation

Validation is being approached in several ways: (i) collocation with higher resolution aircraft data, (ii) ground-based and aircraft in situ observations, and (iii) intercomparisons with other AM-1 platform instruments (especially CALIOP in the A-train). Our validation approach relies heavily on the sources of the data that were used in the algorithm development, which

consisted primarily of the MAS, a fifty channel visible, near-infrared, and thermal infrared imaging spectrometer with 50 m resolution at nadir (cf. King et al. 1996), HIS, a 2 km resolution nadir-viewing Michelson interferometer (later replaced by SHIS, a scanning version) with 0.5 cm^{-1} spectral resolution from 4 to 15 μm (Revercomb et al. 1988), AVIRIS, a 224 band imaging spectrometer from 0.4-2.5 μm with 20 m resolution at nadir, and CPL, a dual polarization nadir viewing lidar (McGill et al. 2002).

Well-calibrated radiances are essential for the development of accurate algorithms. The calibration of the HIS is such that it serves as a reference for line-by-line radiative transfer models. The MAS infrared channels are calibrated through two onboard blackbody sources that are viewed once every scan. Calibration of the shortwave infrared and thermal infrared channels is routinely assessed through vicarious calibration and intercomparisons with the HIS flying on the same aircraft. The MAS solar channels are calibrated in the laboratory, using a 30" integrating sphere before and after each ER-2 deployment, as well as a 20" integrating hemisphere shipped to the field deployment site for calibration trending during deployments. A comprehensive description of both the shortwave and longwave calibration procedures, signal-to-noise characteristics, and thermal vacuum characterization of the MAS can be found in King et al. (1996).

3.2.3.a Field Campaigns

Several field campaigns were planned with the ER-2 aircraft carrying the MAS and HIS (later, SHIS) over various scenes and ecosystems. In addition to the major national and international activities outlined above, we led several focused and short field deployments:

- cold season deployments over the Great Lakes, Hudson Bay, sea ice, and lake ice (based in Madison, WI);
- warm season deployments over the Gulf of Mexico, ARM CART, mountains, and desert (based in Texas or California).

For ARM CART site missions, ground based measurements were included in the data collection. This entailed deployment of the MAS and HIS (SHIS) on the ER-2 aircraft to coincide with a MODIS overflight and to collect simultaneous ground-based class-sondes, AERI (a ground-based Michelson interferometer), tower measurements of temperature and moisture at various

elevations, microwave moisture measurements, lidar and radar cloud observations, and whole sky camera images.

Several field programs have already offered opportunities for pre-launch and post-launch MODIS validation through collection and analysis of observations obtained from MAS, HIS (SHIS), NAST, and CPL. Those field campaigns relating primarily to cloud top properties and cloud phase are found in Table 5.

Table 5. MODIS Field Campaigns used in Cloud Properties Validation

Mission	***Dates***	***Responsible Team Members***	***Primary Purpose***
SUCCESS	April-May 1996	Si-Chee Tsay, Steve Ackerman, Steve Platnick	cirrus cloud properties with MAS and HIS
WINCE	February 1997	Paul Menzel, Steve Ackerman, Dorothy Hall	cloud detection and properties over snow/ice covered land and lakes with MAS and HIS
FIRE III	April-June 1998 August 1998	Michael King Si-Chee Tsay	arctic stratus clouds over sea ice with MAS, HIS
WINTEX	March 1999	Paul Menzel, Steve Ackerman, Bill Smith	atmospheric sounding and cloud/snow detection in winter MAS, SHIS, NAST
WISC-T2000	March 2000	Paul Menzel, Steve Ackerman	First assessment of Terra MODIS radiometric performance with MAS, SHIS, CPL
TX-2001	March – April 2001	Paul Menzel, Steve Ackerman	Radiometric assessment of Terra MODIS with MAS, SHIS
TX-2002	November – December 2002	Paul Menzel, Steve Ackerman	L1B and Cloud properties assessment of Terra and Aqua MODIS with MAS, SHIS, and CPL
Thorpex PTOST	February-March 2003	Steve Ackerman, John Murray, Bill Smith	Atmosheric profiles, cloud properties for Aqua MODIS with MAS, SHIS, NAST, CPL

The Subsonic Aircraft Contrail and Cloud Effects Special Study (SUCCESS) field experiment in April-May 1996 had the goal of determining the radiative properties of cirrus contrails, and to contrast them with naturally occurring cirrus. To assess the radiative impact of these clouds requires a well-calibrated set of radiation measurements and "ground (or in situ) truth" observations. During SUCCESS several MAS and HIS multispectral observations from the NASA ER-2 aircraft were coordinated with in situ aircraft and ground based measurements. The MAS and HIS measurements address the very important relationship between cirrus

radiative properties and the thermodynamic environment (atmospheric temperature and moisture conditions) wherein cirrus clouds form and are maintained. The HIS provides accurate measurements of the atmospheric thermodynamical properties supporting the cirrus life cycle and the MAS measures the cirrus areal extent and radiative properties. Special emphasis has been placed on developing and validating methods of detecting upper tropospheric clouds and defining their areal extent with infrared (e.g. 13.9 μm) and near infrared (e.g. 1.88 μm) channels; these are similar to the MODIS channels and MAS cirrus detection has direct relevance to the MODIS cloud mask algorithm.

Several studies have demonstrated the sensitivity of spectral radiances to cloud particle size and shape distributions. The MAS and HIS instruments provide accurate spectral measurements that can be used to assess differences in the radiative signatures between contrails and naturally occurring cirrus clouds. One difficulty in assessing the impact of high-altitude subsonic aircraft on cirrus formation and modification is the natural variability of the atmosphere and the potentially small signal of the radiative perturbation. Variations in the atmospheric spectral properties for contrail and natural cirrus conditions have been assessed with the two ER-2 instruments in conjunction with in situ and ground-based observations.

The Winter Cloud Experiment (WINCE January-February 1997) was a first investigation into the difficulties of detecting cloud and estimating their properties in winter conditions. Cirrus and thin clouds over frozen tundra and lakes in the northern USA and Canada were measured with the MAS and HIS (along with the GOES-8 and AVHRR). One of the missions investigated the product stability in the transition from day (visible plus infrared) to night (infrared only) and then nighttime only. In addition two ground sites in New England were instrumented for snow and ice cover measurements and MAS/HIS flights were made in clear sky condition (in collaboration with Dorothy Hall and George Riggs working on the MODIS snow/ice product). The field campaign centered in Madison. Examples of the MAS cloud mask were distributed to science team members.

FIRE, the First ISCCP (International Satellite Cloud Climatology Project) Regional Experiment, has previously conducted four successful field missions focused on cloud remote sensing and modeling studies as they relate to climate. FIRE Phase III was conducted in the Arctic in two phases, phase I to be conducted over a 7 week period or longer with a serial deployment of low- to mid-level aircraft, together with a 4 week period of high-altitude ER-2

overflights. During this component of FIRE III, the University of Washington CV-580 and, to a lesser extent, the NCAR C-130Q were utilized. Both of these aircraft were equipped with an extensive set of PMS cloud microphysics probes, a Gerber PVM-100A liquid water content and effective radius probe, Johnson-Williams and King hot wire probes, a Nd:YAG lidar, thermodynamic state variable measurements, and selected chemistry instrumentation. In addition, the ER-2 participated as the upper level aircraft from May 18-June 9, with the MAS, HIS, CLS lidar, a radiation measurement system for radiative fluxes, a multispectral along-track scanning radiometer, and a microwave imaging radiometer. The primary sensors of interest to Goddard Space Flight Center (Michael King, Si-Chee Tsay, Steve Platnick, Robert Pincus) are the MAS on the ER-2, the CAR on the CV-580, and numerous in situ microphysics probes that are invaluable in accessing the accuracy of cloud retrievals of the microphysical and radiative properties of Arctic stratus clouds over a bright (sea ice) surface. This valuable data set has also been of interest to the University of Wisconsin for testing the cloud mask algorithm, cloud phase and cloud top properties.

The first EOS-targeted campaign after the Terra MODIS launch was the WISC-T2000 field campaign. During WISC-T2000, the ER-2 overflew clear scenes of the Great Lakes for L1B validation, and cloudy scenes for cloud properties and cloud detection both in the upper Midwest and over the ARM CART site in Oklahoma. The ER-2 with MAS, SHIS, and CPL were deployed to synchronize with the MODIS overflight; the ARM site suite of ground-based measurements (class-sonde, AERI, tower measurements of temperature and moisture at various elevations, microwave moisture measurements, lidar and radar observations, whole ski images) were collected simultaneously. These measurements were useful to obtain a first assessment of MODIS radiance measurements and geophysical parameters as well. Lidar and radar observations of cloud boundaries over the ARM sites are useful to validate the presence of a cloud as well as its cloud top pressure altitude. Whole sky imagers were also available at the site to compare satellite and ground-based estimates of cloud amount. Finally, optical depth measurements derived from lidar aid in specifying the limit of thin cirrus detection in the cloud mask algorithm and for cloud properties.

The TX-2001 field campaign was designed to do an indepth assessment of Terra MODIS L1B radiometric performance. This effort collected simultaneous MODIS and MAS, SHIS data over clear scenes of the Gulf of Mexico. Targets were selected to include different scan angles

from Terra so that insight could be gained on MODIS scan mirror characterization. This effort showed that the MODIS LWIR cloud phase bands at 8.6um 11um and 12um were indeed well calibrated, complementing first such results from the SAFARI-2000 field program. TX-2001 also showed that the LWIR CO2 bands were however performing too warm, launching an effort that ultimately resulted in an adjustment to the radiometry of these bands for the cloud top properties algorithm.

The TX-2002 field program utilized the MAS, SHIS, NAST, and CPL instruments on the ER-2 for assessing the Aqua MODIS L1B radiometric performance and for assessing the Terra MODIS cloud properties products. Flights over the Gulf of Mexico were used for L1B validation and cloud products assessment. The ER-2 also overflew the ARM CART site in Oklahoma with simultaneous ground based lidar and other ground based instrumentation. These data sets first demonstrated the high quality of Aqua MODIS L1B radiometric performance; however they showed that the LWIR CO2 bands on Aqua also were warmer than expected. The data collection also showed that the Terra MODIS cloud top pressure retrievals tended to be too low in the atmosphere, an important confirmation that continues to be used.

The THORPEX PTOST field effort took place out of Hawaii in February-March 2003 with the MAS, SHIS, CPL, and NAST instruments on the ER-2. These flights were targeted towards validating Aqua MODIS cloud products as well as early GLAS performance. High quality data sets over the Pacific Ocean for a wide range of cloud conditions (single layer thin and thick, multilayer, mid layer, mixed phase, etc.) made this one of the richest data sets collected for cloud product assessment. These data sets have been used to demonstrate that adjustments to the cloud properties algorithms improved the cloud height estimates. The data set also gave a first look into the performance of the cloud phase algorithm, particularly in the challenging environment of mixed phase clouds.

An independent ground validation campaign of MODIS cloud heights is being undertaken through comparisons with stereo determinations of cloud heights (using the MISR over Great Britain and two GOES satellites over the U. S.), aircraft reports of cirrus cloud heights (from the ACARS), and lidar estimates of cirrus heights (using the University of Wisconsin lidar). These intercomparisons have led to useful comparisons between MISR and MODIS cloud detection and cloud heights. Validation of the MODIS cloud emissivity is being attempted through comparison with the lidar determinations. Pre-launch validations came from

cloud top property determinations with MAS data from several field campaigns which included lidar measurements.

Other field campaigns reaching outside the scope of the cloud properties have been conducted. These supply useful data at times for cloud product assessment, particularly when these campaigns are conducted in different environments/climate regions of the World. Table 6 shows some of these. This indicates the intention for an ongoing Cal / Val activity.

Table 6: **Calibration and Validation Field Campaigns**

Name	**Reference URL**	**Principal Airborne Sensors**	**Primary Purpose**
SAFARI-2000	safari.gecp.virginia.edu	MAS, SHIS, CPL, AirMISR	Biophysical validation, LST, VI, Albedo, Aerosol, Fire
BOREAS	boreas.gsfc.nasa.gov/html_pages/boreas_home.html		Biophysical validation, LST, VI, Albedo, Aerosol, Fire
LBA	www-eosdis.ornl.gov/lba_cptec/indexi.html	MAS	Biophysical validation, LST, VI, Albedo, Aerosol, Fire
CLAMS	snowdog.larc.nasa.gov/cave/cave2.0/CLAMS.dir/index.html	NAST-I, NAST-M, MAS	Aerosols
CRYSTAL		MAS, SHIS, NAST, CPL	4-D water vapor fields. Convective initiation. Cirrus properties
THORPEX ATOST	www.nrlmry.navy.mil/~langland/THORPEX_document/Thorpex_plan.htm	MAS, SHIS, NAST, CPL	Atmospheric water vapor and atmospheric turbulence associated with jet streaks
CAMEX	ghrc.msfc.nasa.gov/camex3/instruments/lase.html	MAMS, EDOP	Tropical storm structure
ACE-1 ACE-2	saga.pmel.noaa.gov/ace1.html www.ei.jrc.it/ace2		Aerosol, dust transport, RTE

3.2.3.b Using the A-train and other satellite platforms

Comparisons with products from other platforms have also been made. Cloud masks have been compared with those from AVHRR and HIRS/2 data, ASTER and MISR (also on the Aqua platform), and CERES. Atmospheric profiles have been compared with those from HIRS, GOES, and AIRS (also on the Aqua platform). Cloud properties have been intercompared with those derived from HIRS, GOES, CERES, MISR, AIRS, and CALIPSO, as well as from in situ aircraft (see below). Timing, coverage and resolution vary from one instrument to another; for example with ASTER, comparisons are possible for selected swaths (60 km wide with 30 m

resolution) that are available for different (and selected) ecosystems no more than once every 16 days.

CALIPSO (Cloud-Aerosol Lidar and Infrared Pathfinder Satellite Observation) takes measurements about 75 seconds behind that of Aqua MODIS as they both orbit the Earth from pole to pole. Collocation is accomplished by matching the CALIPSO latitude and longitude to those of a 5x5 km MODIS cloud top pressure. Cloud top pressures were converted to heights using the GFS (as indicted above for airborne lidar comparisons) and were compared to heights from analysis of CALIPSO 0.532-μm backscatter data.

3.2.3.c Validation of Cloud Top Properties Algorithm

The following discussion is taken from Baum et al. (2012). MODIS and CALIOP collocation files are prepared for data products from each MODIS granule. These collocation files are analyzed subsequently to produce global comparison statistics. Figure 12a shows the gridded mean values of the (MODIS C5 – CALIOP) CTH differences for the month of August, 2006, at 5˚ resolution in latitude and longitude between 60˚N–60˚S, with both sensor products at 5-km spatial resolution. The (MODIS C5 – CALIOP) CTH differences are limited to single-layered clouds as determined by CALIOP. Similar results are provided in Fig. 12b for (MODIS C6– CALIOP) CTH values. The most notable improvement in the (MODIS C6–CALIOP) CTH comparison (Figure 12b) is the reduction in positive values of (MODIS–CALIOP) CTH differences – this is a result of applying the new lapse–rate approach for estimating low cloud CTH in the MODIS data (Holz et al., 2008). The non-polar low cloud height (CALIOP CTH < 3 km) bias of 424 m for Collection 5 was reduced to 197 m for Collection 6.

Another way of comparing the MODIS and CALIOP CTH is provided in Figure 13, which shows the CTH differences between the MODIS C5/C6 and CALIOP products, again with both sensor products at 5-km spatial resolution. The percentages are calculated at 0.1–km CTH difference resolution; integration of the percentages in each panel sums to 100%. Fig. 13a filters the total number of MODIS and CALIOP match-ups for the month of August, 2006, between 60˚N-60˚S for single-layered cirrus over both ocean and land. The single-layered cirrus is defined when two conditions are met: (a) CALIOP CTH ≥ 8km and (b) CALIOP sees the surface. For this month, a total of 54,992 MODIS–CALIOP collocations met these conditions. There are two features to note in Fig 13a. First, the (MODIS–CALIOP) CTH differences

occurring between -7 and -12 km (i.e., high cloud being miscast as low cloud by MODIS) decreased for the C6 product. Second, the peak for C6 near a value of -1km is higher than for the C5 results. Some differences in (MODIS-CALIOP) CTH are expected since MODIS sees into the cloud to an optical thickness of approximately one while CALIOP senses the cloud top (Holz et al. 2008). Together, these results indicate that CO_2 slicing is being used more often, and to greater advantage, with the C6 algorithm than occurred with C5.

3.2.3.d Validation for Cloud Phase Algorithm

An evaluation of the IR phase results is provided through comparison with CALIOP Version 3 cloud products using the new phase algorithm in Hu et al. (2009). A comparison of IRP for co-located MODIS and CALIOP products is presented in Fig. 14. The results shown provide the likelihood of inferring water/ice phase as a function of CALIOP mean cloud temperature, following the approach shown in Giraud et al. (2001, see Figure 12). The Giraud et al. (2001) study is based on collocated products from POLDER (POLarization and Directionality of the Earth's Reflectance) and ATSR-2 (Along Track Scanning Radiometer). POLDER data provide the cloud thermodynamic phase following Riedi et al. (2000) and the ATSR-2 data are analyzed to provide the cloud top temperature (CTT). Their results over ocean indicated that the likelihood of finding ice clouds is less than 5% for CTT $\geq$ 268K, and greater than 95% for CTT $\leq$ 238K. As CTT decreases from 268K to 238K, the likelihood of finding an ice cloud increases following a nearly linear relationship.

The cloud products are filtered so that results are shown only for collocations where CALIOP data indicate single-layered clouds and an optical thickness $\tau \geq 0.5$. At each CALIOP mean cloud temperature, the CALIOP or MODIS cloud phase retrievals at that temperature are normalized so that the percentages of each category (water, ice, and uncertain) sum to 100%. Figs. 14a and 14b show the results from CALIOP for ocean and land respectively. The CALIOP ice-water phase confidence flags were not used to filter the results – all data were used. After filtering the CALIOP results for single-layered clouds and leaving out the most optically thin clouds, there are only a few percent of uncertain retrievals in the CALIOP Version 3 products except at warm cloud temperatures above 285K over land. This indicates that CALIOP is able to infer the presence of ice or water clouds fairly unambiguously. Over both land and ocean, it is somewhat surprising to find that CALIOP infers the presence of a high percentage of water

clouds even at cloud temperatures below 250K. These results are supported by Hu et al. (2010) in a study of supercooled water clouds using CALIOP data. Over land, where there tend to be higher concentrations of ice nuclei (IN), the percentage of supercooled water clouds decreases with mean cloud temperature in comparison with the results over ocean.

In comparison with the CALIOP results, the MODIS C6 results shown in Figs. 14c and 14d over ocean and land, respectively, both indicate much higher percentages of pixels for which the cloud phase retrieval is uncertain, especially between 240K and 260K. While the improvements in the MODIS cloud phase algorithm presented in this study pertain mostly to optically thin ice clouds, the ability to infer the presence of supercooled water clouds remains an issue using only IR bands (Nasiri and Kahn 2008; Cho et al. 2009). The results for MODIS are provided as a function of CALIOP mean cloud temperature, not optical thickness; the results include retrievals over a range of cloud optical thicknesses. It should be noted that the use of the emissivity ratios over land for the MODIS cloud phase are influenced to some degree by the quality of the surface temperature provided by the meteorological model product. The clear-sky radiative transfer model incorporates the global surface emissivity database in Seeman et al. (2008).

3.2.4.a Quality Control of Cloud Top Properties Algorithm

As indicated in section 3.1.3.a., the accuracy of the cloud top pressures have been found to be 50 hPa root mean square with respect to radiosonde, stereo, and lidar estimates; the effective emissivity determinations have been found to be correlate within 20% root mean square of lidar visible estimates of optical thickness.

Quality control within the software checks for cloud forcing greater than the instrument noise and cloud top pressure within the atmospheric layer where temperature and pressure enjoy a one to one relationship. Additionally, cloud top pressures are stratified as a function of satellite viewing angle to make sure that the atmospheric transmittance corrections for viewing angle are not introducing a bias.

Beyond these simple tests, quality control is accomplished by manual and automated inspection of the data and comparison to other sources of cloud information. MODIS cloud top pressures and effective emissivities are being compared to those determined from the NOAA HIRS and the GOES sounder. Additional data from field experiments using the MODIS Airborne Simulator on the ER2 assists with quality assessment of the MODIS cloud parameter determinations.

Global mean distributions of cloud height and emissivity are being compared from one week to the next; thresholds are set to flag unrealistic changes. Trend analyses of global cloud properties are being compared with trends in OLR; a strong correlation between the two is being realized. Additionally comparisons with ISSCP are being made. These comparisons are all done with the gridded 1.0 degree resolution MODIS cloud properties (determined from averaging of the 5 x 5 pixel cloud properties).

The cloud top properties and cloud phase product (the 5 km resolution part of MOD06) carry 10 bytes of quality analysis information for each pixel. The information contained in this byte array include a confidence in the usefulness of each individual parameter, input data resource flags and processing path flags. Please refer to the MODIS Atmosphere QA Plan for exact details.

3.2.4.b Quality Control of Cloud Phase Algorithm

Quality control includes consistency checks with previous days resultant statistics, including the global cloud phase determination consistency and known cloud area persistence consistency (marine stratus regions, etc.).

The cloud top properties and cloud phase product (the 5 km resolution part of MOD06) carry 10 bytes of quality analysis information for each pixel. The information contained in this byte array includes a confidence in the usefulness of each individual parameter, input data resource flags and processing path flags. The MODIS Atmosphere QA Plan provides details.

3.2.5 Exception Handling

If the required radiance data is not available, then the algorithm records the cloud products missing for that 5 x 5 pixel area.

3.2.6.a Data Dependencies of Cloud Top Properties Algorithm

The CO_2 slicing algorithm needs calibrated, navigated, coregistered one km FOV radiances from channels 29 (8.6 micron for moisture correction), 31 (11.03 micron infrared window), 32 (12.02 micron for moisture correction), 33-36 (13.335, 13.635, 13.935, and 14.235 microns CO_2 absorption band channels). Navigation implies knowledge of the surface terrain including height (DEM) and whether land or sea. The MODIS viewing angle for a given FOV must be known. The cloud mask from visible and infrared radiance considerations is used as a

indicator for cloud cover within a given one km FOV. The NCEP GDAS Final Run global model analysis of surface temperature and pressure as well as profiles of temperature and moisture are initially used in the calculation of the cloud forcing as a function of pressure and effective emissivity (in Equation (3)); AIRS/AMSU profiles are also used. The Reynolds blended SST is also used over the ocean. The algorithm also requires knowledge of the clear radiances for evaluation of the cloud forcing for each channel used in the ratio tests. This information is provided in the form of clear radiance maps created and updated daily by the cloud mask production software. Table 7 summarizes the input data dependencies.

There has been some consideration for using the short wavelength CO_2 spectral bands 22 through 25 in parallel with the long wavelength CO_2 bands in a composite CO_2 slicing algorithm. The shortwave CO_2 algorithm has problems with reflected solar contributions during daylight hours, but is useful additional information at night. Current plans do not include these bands, but future versions of the software might.

Table 7. **MODIS Cloud Parameter Input Data Dependencies**

MODIS data channels	29, 31-36
Navigation	lat, lon, land, sea
MODIS viewing angle	lin, ele, ang
Cloud mask	yes, no, type
Surface data	SST, model analysis of temperature, dewpoint and pressure, topography (DEM)
Model profiles	temp (12 levels), moisture (6 levels)
Clear Radiance Base Maps	Channels 31, 33-36.

Table 8. **MODIS Cloud Phase Input Data Dependencies**

MODIS data channels	28, 29, 31, 32
MODIS cloud mask	cloud or clear
Navigation	lat, lon, land, sea
MODIS viewing angle	lin, ele, ang
Surface data	SST, model analysis of temperature, dewpoint and pressure, surface emissivity topography (DEM)
Model profiles	temp, relative humidity

Table 9. **MODIS cloud product (MOD06 - 5 km) Output File Contents**

parameter type	Bytes	content
double	8	Scan Start Time
float	4	location latitude
float	4	location longitude
short	2	Solar Zenith Angle
short	2	Solar Azimuth Angle
short	2	Sensor Zenith Angle
short	2	Sensor Azimuth Angle
short	14	brightness temperature of bands 29,31-36
short	2	surface temperature
short	2	surface pressure
byte	1	processing flag
byte	1	cloud height method (CO_2 slicing or IR window)
short	2	cloud top pressure
short	2	cloud top pressure day
short	2	cloud top pressure night
short	2	cloud top temperature
short	2	cloud top temperature day
short	2	cloud top temperature night
short	2	tropopause height
byte	1	cloud fraction
byte	1	cloud fraction day
byte	1	cloud fraction night
byte	1	cloud effective emissivity
byte	1	cloud effective emissivity day
byte	1	cloud effective emissivity night
short	2	cloud top pressure from IR window
short	2	spectral cloud forcing
short	10	cloud top pressure from ratios (33/31, 34/33, 35/33, 35/34, 36/35)
short	2	surface type
short	14	radiance variance (7 channels)
short	4	brightness temperature difference (8-11, 11-12)
byte	1	cloud phase infrared
byte	1	cloud phase infrared day
byte	1	cloud phase infrared night
byte	10	quality assurance at 5x5 km resolution

Total: 111 bytes/pixel

Table 10. **Cloud Top Property and Cloud Phase Level 3 Output File Contribution to Joint Atmosphere Level 3 Products**

parameter number	content
1	thermodynamic phase (coded 0-6)
2	thermodynamic phase (coded 0-6) day
3	thermodynamic phase (coded 0-6) night
4	cloud top temperature
5	cloud top temperature day
6	cloud top temperature night
7	cloud top pressure
8	cloud top pressure day
9	cloud top pressure night
10	cloud top effective emissivity
11	cloud top effective emissivity day
12	cloud top effective emissivity night
13	probability of cirrus
14	probability of high cloud

3.2.6.b Data Dependencies of Cloud Phase Algorithm

The bispectral cloud phase algorithm needs calibrated, navigated, coregistered one km FOV radiances (for FOV uniformity screening and conversion to brightness temperatures) from channels 29 (8.6 micron) and 31 (11.03 micron). The MODIS viewing angle for a given FOV must be known. The MODIS cloud mask product is used to screen areas where the probability of cloud is high. A global surface emissivity map (related to surface cover) is used to adjust ice/water thresholds. Table 8 is a summary of the input data dependencies.

3.2.7.a Level 2 Output Product of Cloud Top Properties and Cloud Phase Algorithm

The Level 2 output file for each 5 x 5 pixel area (when cloud is present) is summarized in Table 9. The combined MODIS cloud properties, cloud phase and cloud retrieval product number is MOD06 (Terra) and MYD06 (Aqua).

3.2.7.b Level 3 Output Product of Cloud Top Properties and Cloud Phase Algorithm

The Level 3 cloud top properties and cloud phase products are included as part of a joint atmosphere discipline group product (MOD44). The products are produced on a daily bases from the Level 2 files, on an 8 day basis from the daily files and a monthly bases from the daily Level 3 files. The Level 3 daily files are produced at 1.0 degree equal area only, while the 8 day and monthly Level 3 product files are produced for both 1.0 degree equal area and 1.0 degree equal angle grids. The cloud top properties and cloud phase contribution to the joint product is shown in Table 10.

3.3 References

Ackerman, S. A., W. L. Smith and H. E. Revercomb, 1990: The 27-28 October 1986 FIRE IFO cirrus case study: spectral properties of cirrus clouds in the 8-12 micron window. Mon. Wea. Rev., 118, 2377-2388.

Ackerman, S. A., R. E. Holz, R. Frey, E. W. Eloranta, B. C. Maddux, and M. McGill, 2008: Cloud detection with MODIS. Part II: Validation, *J. Atmos. Oceanic Tech.*, **25**, 1073-1086.

Baum, B. A., D. P. Kratz, P. Yang, S. Ou, Y. Hu, P. F. Soulen, and S-C. Tsay, 2000a: Remote sensing of cloud properties using MODIS Airborne Simulator imagery during SUCCESS. I. Data and models. *J. Geophys. Res.*, **105**, 11,767-11,780.

Baum, B. A., P. F. Soulen, K. I. Strabala, M. D. King, S. A. Ackerman,W. P. Menzel, and P. Yang, 2000b: Remote sensing of cloud properties using MODIS Airborne Simulator imagery during SUCCESS. II. Cloud thermodynamic phase. *J. Geophys. Res.*, **105**, 11,781-11,792.

Baum, B. A., W. P. Menzel, R. A. Frey, D. Tobin, R. E. Holz, Ackerman, S. A., A. K. Heidinger, and P. Yang, 2012: MODIS cloud top property refinements for Collection 6. *J. Appl. Meteor. Clim.*, **51**, 1145-1163.

Booth, A. L., 1973: Objective cloud type classification using visual and infrared satellite data. 3rd Conference on Probability and Statistics in the Atmospheric Sciences. Am. Meteor. Soc., Boulder, CO.

Chahine, M. T., 1974: Remote sounding of cloudy atmospheres. I. The single cloud layer. J. Atmos. Sci., 31, 233-243.

Cho H.-M., S. L. Nasiri, and P. Yang, 2009: Application of CALIOP measurements to the evaluation of cloud phase derived from MODIS infrared channels. *J. Appl. Meteorol. Clim.*, **48**, 2169-2180.

Downing, H. D., and D. Williams, Optical constants of water in the infrared, *J. Geophys. Res.*, *80*, 1656-1661, 1975.

Eyre, J. R., and W. P. Menzel, 1989: Retrieval of cloud parameters from satellite sounder data: A simulation study. J. Appl. Meteor., 28, 267-275.

Gao, B.-C. and W. J. Wiscombe, 1994: Surface-induced brightness temperature variations and their effects on detecting thin cirrus clouds using IR emission channels in the 8-12 micron region. J. Appl. Met., 33, 568-570.

Giraud, V., O. Thouron, J. Riedi, and P. Goloub, 2001: Analysis of direct comparison of cloud top temperature and infrared split window signature against independent retrievals of cloud thermodynamic phase. *Geophys. Res. Lett*., **28**, 983-986.

Gruber, A., and T. S. Chen, 1988: Diurnal variation of outgoing longwave radiation. J. Clim. Appl. Meteor., 8, 1-16.

Heidinger, A. K.; M. J. Pavolonis, R. E. Holz, B. A. Baum, and S. Berthier, 2010: Using CALIPSO to explore the sensitivity to cirrus height in the infrared observations from NPOESS/VIIRS and GOES-R/ABI. *J. Geophys. Res*., **115**, doi:10.1029/2009JD012152.

Heidinger, A. K. and M. J. Pavolonis, 2009: Gazing at cirrus clouds for 25 years through a split window, part 1: Methodology. *J. Appl. Meteorol. Clim* , **48**, 2009, pp.1100-1116.

Holz, R. E., S. A. Ackerman, F. W. Nagle, R. Frey, S. Dutcher, R. E. Kuehn, M. Vaughan, and B. A. Baum, 2008: Global MODIS cloud detection and height evaluation using CALIOP. *J. Geophys. Res*., **113**, D00A19, doi:10.1029/2008JD009837.

Hu, Y.-X., D. Winker, M. Vaughan, B. Lin, A. Omar, C. Trepte, D. Flittner, P. Yang, S. L. Nasiri, B. A. Baum, W. Sun, Z. Liu, Z. Wang, S. Young, K. Stamnes, J. Huang, R. Kuehn, and R. E. Holz, 2009: CALIPSO/CALIOP cloud phase discrimination algorithm. *J. Atmos. Ocean. Technol.*, **26**, 2293-2309.

Hu, Y.-X., S. Rodier, K.-M. Xu, W. Sun, J. Huang, B. Lin, P. Zhai, and D. Josset, 2010: Occurrence, liquid water content, and fraction of supercooled water clouds from combined CALIOP/IIR/MODIS measurements. *J. Geophys. Res*., **115**, D00H34, doi:10.1029/2009JD012384.Menzel, W. P., R. Frey, H. Zhang, D. Wylie, C.

Moeller, R. Holz, B. Maddux, B. A. Baum, K. Strabala, and L. Gumley, 2008: MODIS global cloud-top pressure and amount estimation: algorithm description and results. *J. Appl. Meteor. Climatol.*, **47**, 1175-1198.Inoue, T., 1987: A cloud type classification with NOAA 7 split window measurements. J. Geophys. Res., 92, 3991-4000.

Inoue, T., 1989: Features of clouds over the Tropical Pacific during the Northern Hemispheric winter derived from split window measurements. J. Meter. Soc. Japan, 67, 621-637.

Jacobowitz, H. J., 1970: Emission scattering and absorption of radiation in cirrus clouds. Ph.D. thesis, Massachusetts Institute of Technology, 181 pp.

King, M. D., W. P. Menzel, P. S. Grant, J. S. Myers, G. T. Arnold, S. E. Platnick, L. E. Gumley, S. C. Tsay, C. C. Moeller, M. Fitzgerald, K. S. Brown and F. G. Osterwisch, 1996: Airborne scanning spectrometer for remote sensing of cloud, aerosol, water vapor and surface properties. J. Atmos. Oceanic Technol., 13, 777-794.

King, M. D., Y. J. Kaufman, W. P. Menzel and D. Tanre, 1992: Remote sensing of cloud, aerosol, and water vapor properties from the Moderate Resolution Imaging Spectrometer (MODIS). IEEE Trans. Geosci. Remote Sensing, 30, 2-27.

McGill, M.J., D.L. Hlavka, W.D. Hart, J.D. Spinhirne, V.S. Scott, and B. Schmid, "The Cloud Physics Lidar: Instrument description and initial measurement results", *Applied Optics,* 41, pg. 3725-3734, June 2002.

Menzel, W. P., W. L. Smith, and T. R. Stewart, 1983: Improved cloud motion wind vector and altitude assignment using VAS. J. Clim. Appl. Meteor., 22, 377-384.

Menzel, W. P., D. P. Wylie, and A. H.-L. Huang, 1986: Cloud top pressures and amounts using HIRS CO_2 channel radiances. Technical Proceedings of the Third International TOVS Study Conference, 13-19 August 1986, Madison, WI, 173-185.

Menzel, W. P. and K. I. Strabala, 1989: Preliminary report on the demonstration of the VAS CO_2 cloud parameters (cover, height, and amount) in support of the Automated Surface Observing System (ASOS). NOAA Tech Memo NESDIS 29.

Menzel, W. P., D. P. Wylie, and K. I. Strabala, 1989: Characteristics of global cloud cover derived from multispectral HIRS observations. Technical Proceedings of the Fifth International TOVS Study Conference, 24-28 July 1989, Toulouse, France, 276-290.

Menzel, W. P., D. P. Wylie, and K. I. Strabala, 1992: Seasonal and Diurnal Changes in Cirrus Clouds as seen in Four Years of Observations with the VAS. J. Appl. Meteor., 31, 370-385.

Menzel, W. P., R. A. Frey, H. Zhang, D. P. Wylie., C. C. Moeller, R. A. Holz, B. Maddux, B. A. Baum, K. I. Strabala, and L. E. Gumley, 2008: MODIS global cloud-top pressure and amount estimation: algorithm description and results. *Jour of App Meteor and Clim*., **47**, 1175-1198.

Nasiri, S. L. and B. H. Kahn, 2008: Limitations of bi-spectral infrared cloud phase determination and potential for improvement. *J. Appl. Meteorol. Clim.*, **47**, 2895-2910.

Parol, F. J., C. Buriez, G. Brogniez and Y. Fouquart, 1991: Information content of AVHRR Channels 4 and 5 with respect to the effective radius of cirrus cloud particles. J. Appl. Meteor., 30, 973-984.

Pavolonis, M. J., Advances in extracting cloud composition information from spaceborne infrared radiances - A robust alternative to brightness temperatures, part 1: Theory. *J. Appl. Meteorol. Clim.,* **49**, 1992-2012.

Platnick. S., M. D. King, S. A. Ackerman, W. Paul Menzel, B. A. Baum, and R. A. Frey, 2003: The MODIS cloud products: Algorithms and examples from Terra. *IEEE Trans. Geosci, Remote Sens.* **41**, 459-473.

Riedi, J., M. Doutriaux-Boucher, P. Goloub, and P. Couvert, 2000: Global distribution of cloud top phase from POLDER/ADEOS-1. *Geophys. Res. Lett*., **27**, 1707-1710.

Rossow, W. B., and A. A. Lacis, 1990: Global and seasonal cloud variations from satellite radiance measurements. Part II: Cloud properties and radiative effects. J. Clim., in press.

Schmetz, J., S. A. Tjemkes, M. Gube, and L. van de Berg, 1997: Monitoring deep convection and convective overshooting with Meteosat, *J. Adv. Space Res.,* **10**, 433–441.

Seemann, S. W., E. E. Borbas, R. O. Knuteson, G. R. Stephenson, H.-L. Huang, 2008: Development of a global infrared land surface emissivity database for application to clear sky sounding retrievals from multispectral satellite radiance measurements. *J. Appl. Meteor. Climatol.*, **47**, 108–123.

Soden, B. J., and F. B. Bretherton, 1993: Upper tropospheric relative humidity from the GOES 6.7 μm channel: Method and climatology for July 1987. *J. Geophysical Research,* **98**, 16669–16688.

Smith, W. L., H. M. Woolf, P. G. Abel, C. M. Hayden, M. Chalfant, and N. Grody, 1974: Nimbus 5 sounder data processing system. Part I: Measurement characteristics and data reduction procedures. NOAA Tech. Memo. NESS 57, 99pp.

Smith, W. L., and C. M. R. Platt, 1978: Intercomparison of radiosonde, ground based laser, and satellite deduced cloud heights. J. Appl. Meteor., 17, 1796-1802.

Smith, W. L., H. M. Woolf, and H. E. Revercomb, 1991: Linear simultaneous solution of temperature and absorbing constituent profiles from radiance spectra. Appl. Optics, 30, 1117-1123.

Spinhirne, J.D., and W. D. Hart, 1990: Cirrus structure and radiative properties from airborne lidar and spectral radiometer observations. Mon. Wea. Rev., 2329.

Strabala, K. I., S. A. Ackerman and W. P. Menzel, 1994: Cloud properties inferred from 8-12 micron data. Accepted to the J. Appl. Meteor., March 1994 issue.

Susskind, J., D. Reuter, and M. T. Chahine, 1987: Cloud fields retrieved from analysis of HIRS/MSU sounding data. J. Geophys. Res., 92, 4035-4050.

Takano, Y., K. N. Liou and P. Minnis, 1992: The effects of small ice crystals on cirrus infrared radiative properties. J. Atmos. Sci., 49, 1487-1493.

Tobin, D. C., H. E. Revercomb, C. C. Moeller, and T. S. Pagano, 2006: Use of AIRS high spectral resolution infrared spectra to assess the calibration of MODIS on EOS Aqua, *J. Geophys. Res.*, **111**, D09S05, doi:10.1029/2005JD006095.

Warren, S. G., 1984: Optical constants of ice from the ultraviolet to the microwave. Appl. Optics, 23, 1206-1225.

Wielicki, B. A., and J. A. Coakley, 1981: Cloud retrieval using infrared sounder data: Error analysis. J. Appl. Meteor., 20, 157-169.

Wu, M. L. and J. Susskind, 1990: Outgoing longwave radiation computed from HIRS2/MSU soundings. J. Geophys. Res., 95D, 7579-7602.

Wylie, D. P., and W. P. Menzel, 1989: Two years of cloud cover statistics using VAS. J. Clim., 2, 380-392.

Wylie, D. P. and W. P. Menzel, 1991: Two Years of Global Cirrus Cloud Statistics using HIRS. Technical Proceedings of the Sixth International TOVS Study Conference held 1-6 May 1991 in Airlie, VA, 344-353.

Wylie, D. P., W. P. Menzel, H. M. Woolf, and K. I. Strabala, 1994: Four Years of Global Cirrus Cloud Statistics Using HIRS. J. Clim., 7, 1972-1986.

Zhang, H. and W. P. Menzel, 2002: Improvement in Thin Cirrus Retrievals Using an Emissivity Adjusted CO_2 Slicing Algorithm**.** Accepted by Jour. Geophys. Rev.

4.0 Assumptions

4.1 Assumptions of Cloud Top Properties Algorithm

The data are assumed to be calibrated (within the instrument noise), navigated (within one FOV), and coregistered (within two tenths of a FOV). The algorithm assumes the presence of only one cloud layer of infinitesimal thickness; adjustments for the presence of multiple cloud layers are under investigation. The cloud need not cover the entire FOV. Spectral cloud forcing must be greater than the instrument noise. Bias between global forecast model calculated and MODIS measured radiances must be accounted for.

4.2 Assumptions of IR Cloud Phase Algorithm

The data are assumed to be calibrated (within the instrument noise), navigated (within one FOV), and coregistered (within two tenths of a FOV). The C6 1-km algorithm also requires more ancillary data than previously because it requires a clear-sky radiative transfer model, including surface emissivity, temperature/humidity profiles, and surface elevation.

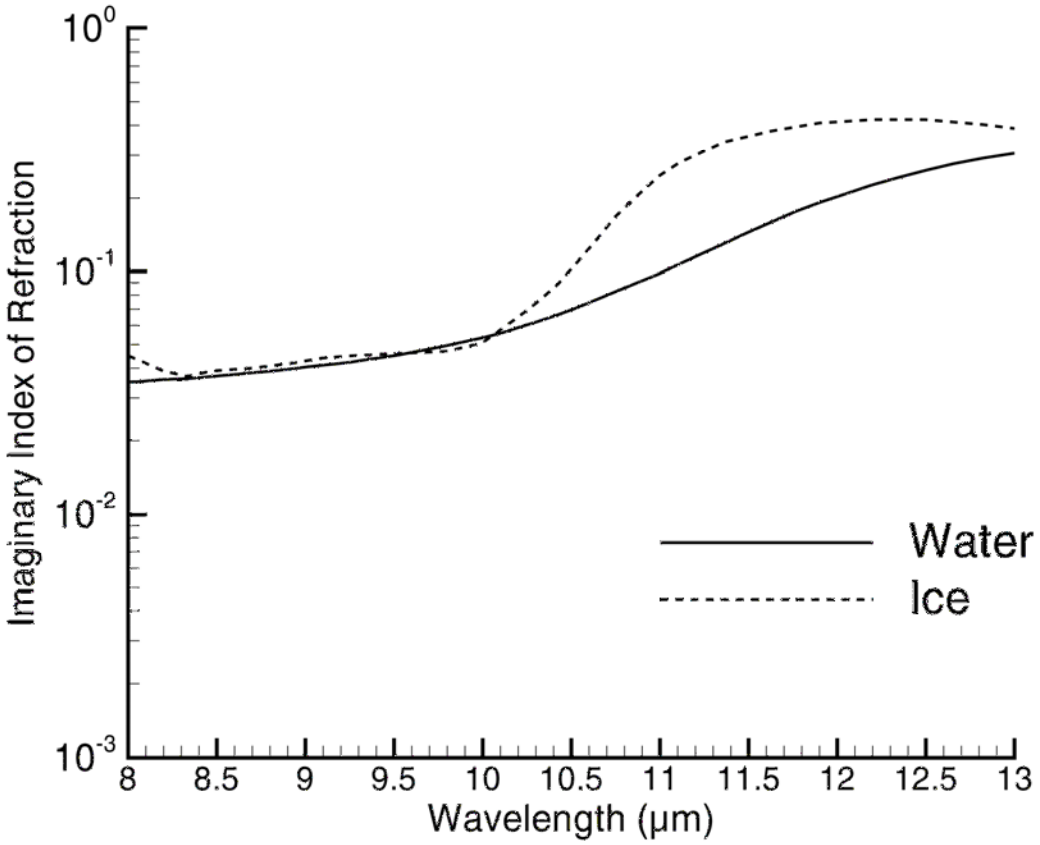

Figure 1: Imaginary index of refraction for water and ice between 8 and 13 μm.

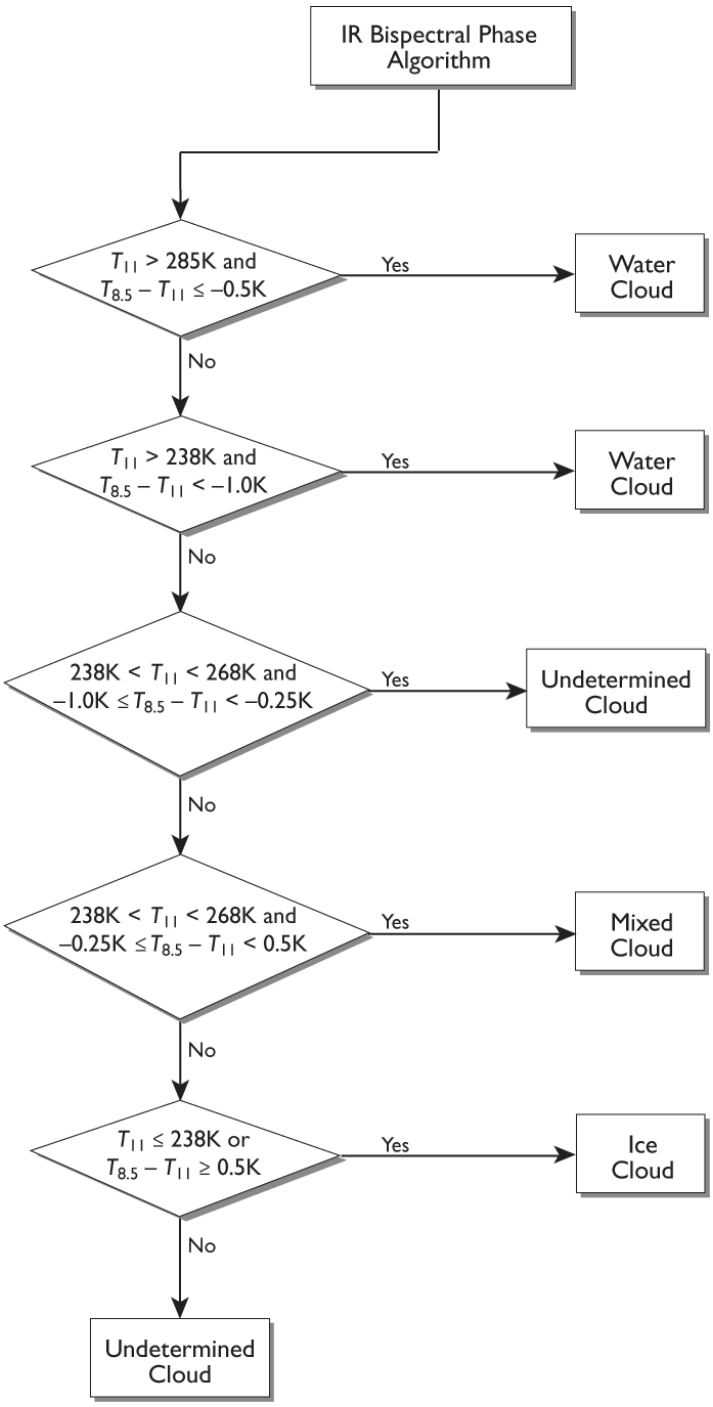

Figure 2: Decision tree for MODIS Collection 6 (and earlier) IR cloud phase determination for 5-km product only. One change for Collection 6: the classes for Undetermined Cloud and Mixed-Phase Cloud are combined into an "uncertain phase" category. Note that the current methodology has static thresholds that are not dependent on the viewing (or scan) angle or surface ecosystem.

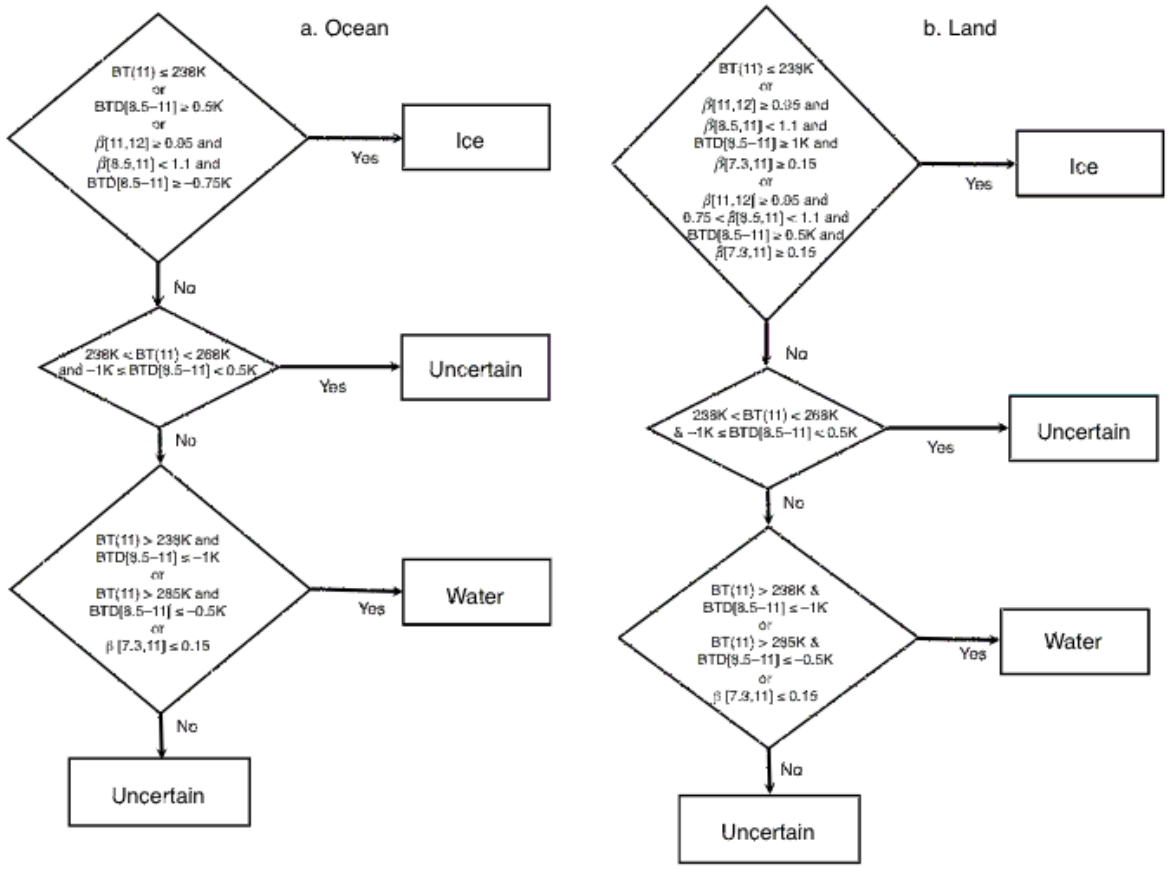

Figure 3: Decision tree for MODIS Collection 6 IR cloud phase determination over (a) ocean and (b) land for the new 1-km product.

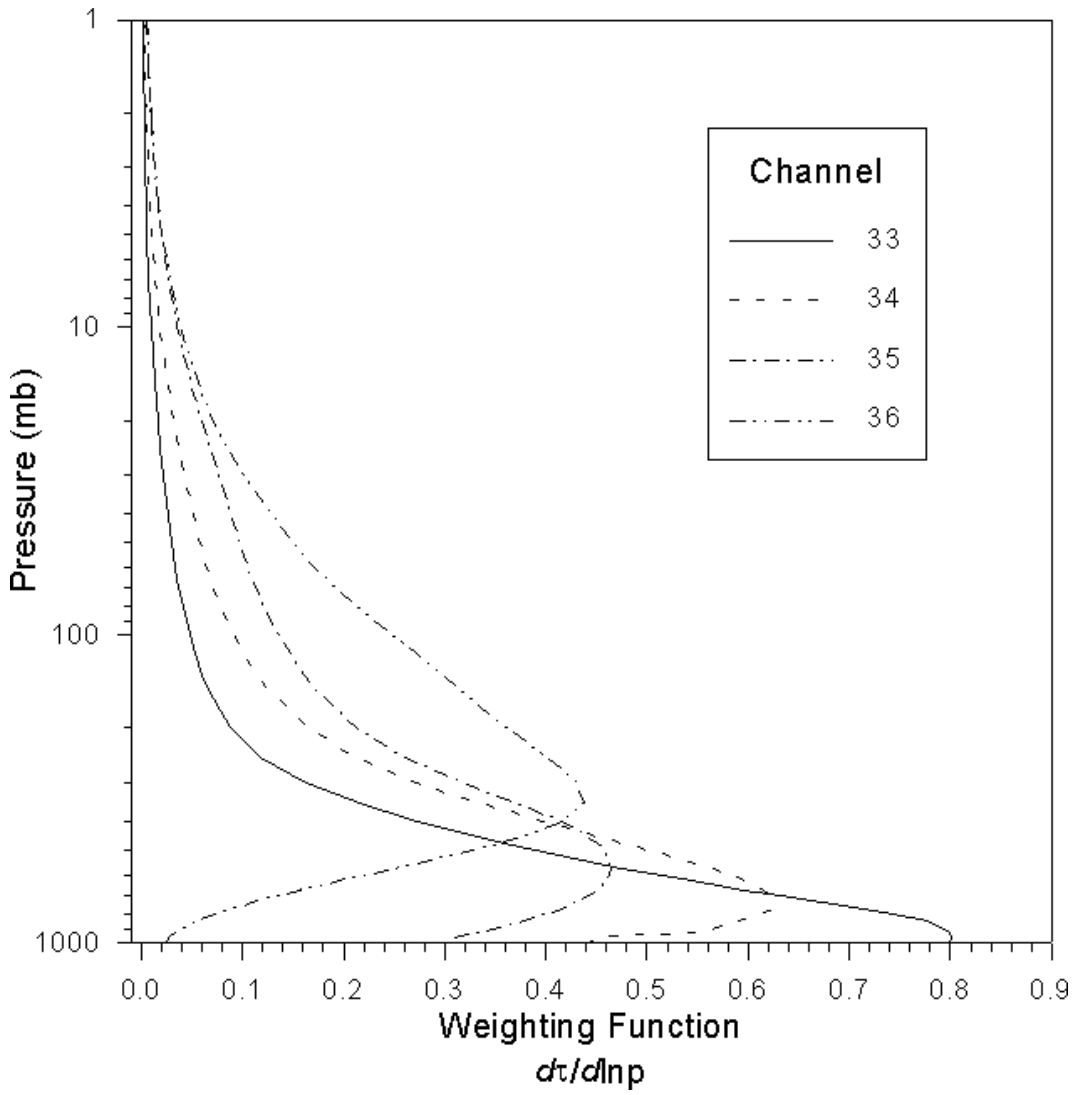

Figure 4. Weighting functions for the four MODIS channels in the CO_2 absorption band

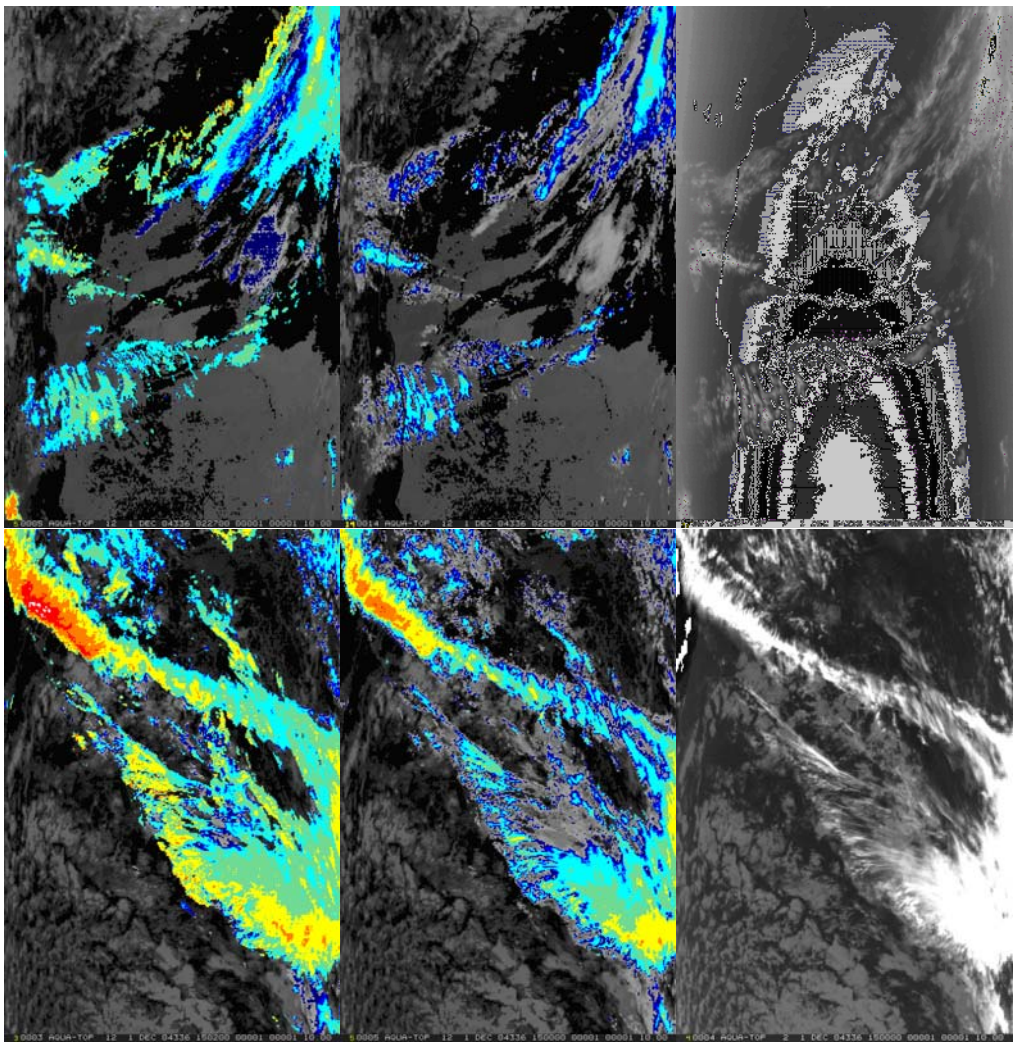

Figure 5: MODIS Aqua CTP results (CTP < 400 in color) for two different scenes on 1 December 2004 after radiance bias adjustment (left panel), before radiance bias adjustment (middle panel), and black and white infrared image of the scene (right panel). White indicates clouds between 95 and 125 hPa, red 125 and 160 hPa, orange160 and 190 hPa, yellow 190 and 225 hPa, aqua 225 and 260 hPa, cyan 260 and 300 hPa, sky 300 and 330 hPa, blue 330 and 360 hPa, and navy 360 and 390 hPa.

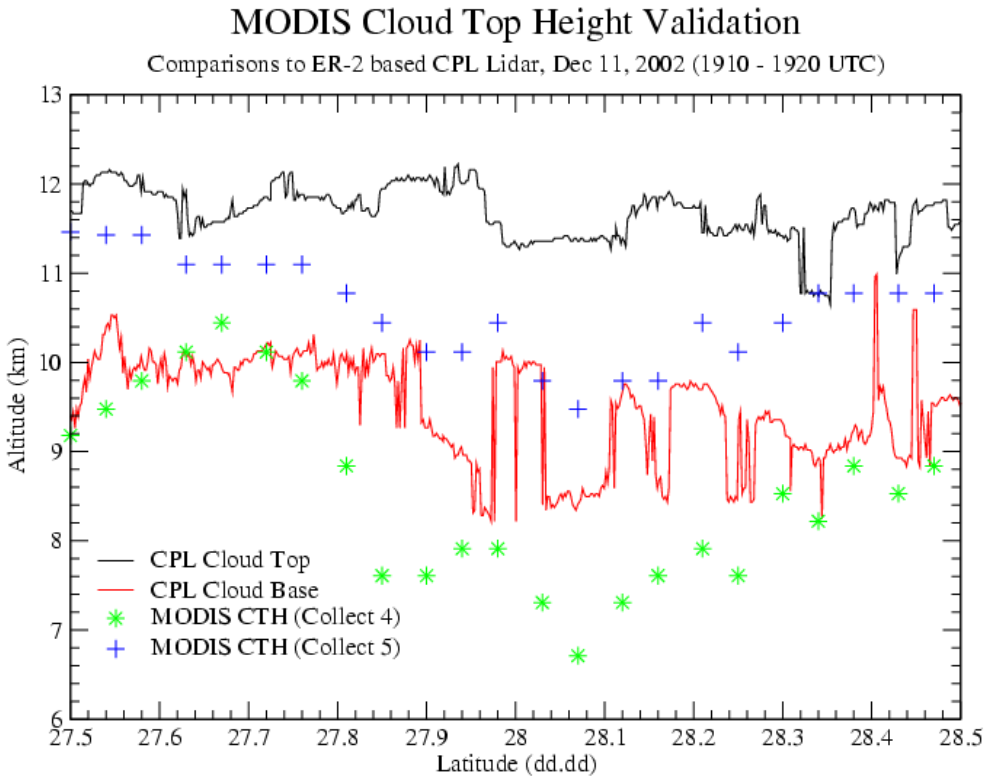

Figure 6. Comparison of Cloud Physics Lidar determinations of cloud top and bottom with the Collect 5 MODIS cloud top heights (inferred from pressure using the Global Forecast System pressure profiles) over cirrus clouds on 11 December 2002.

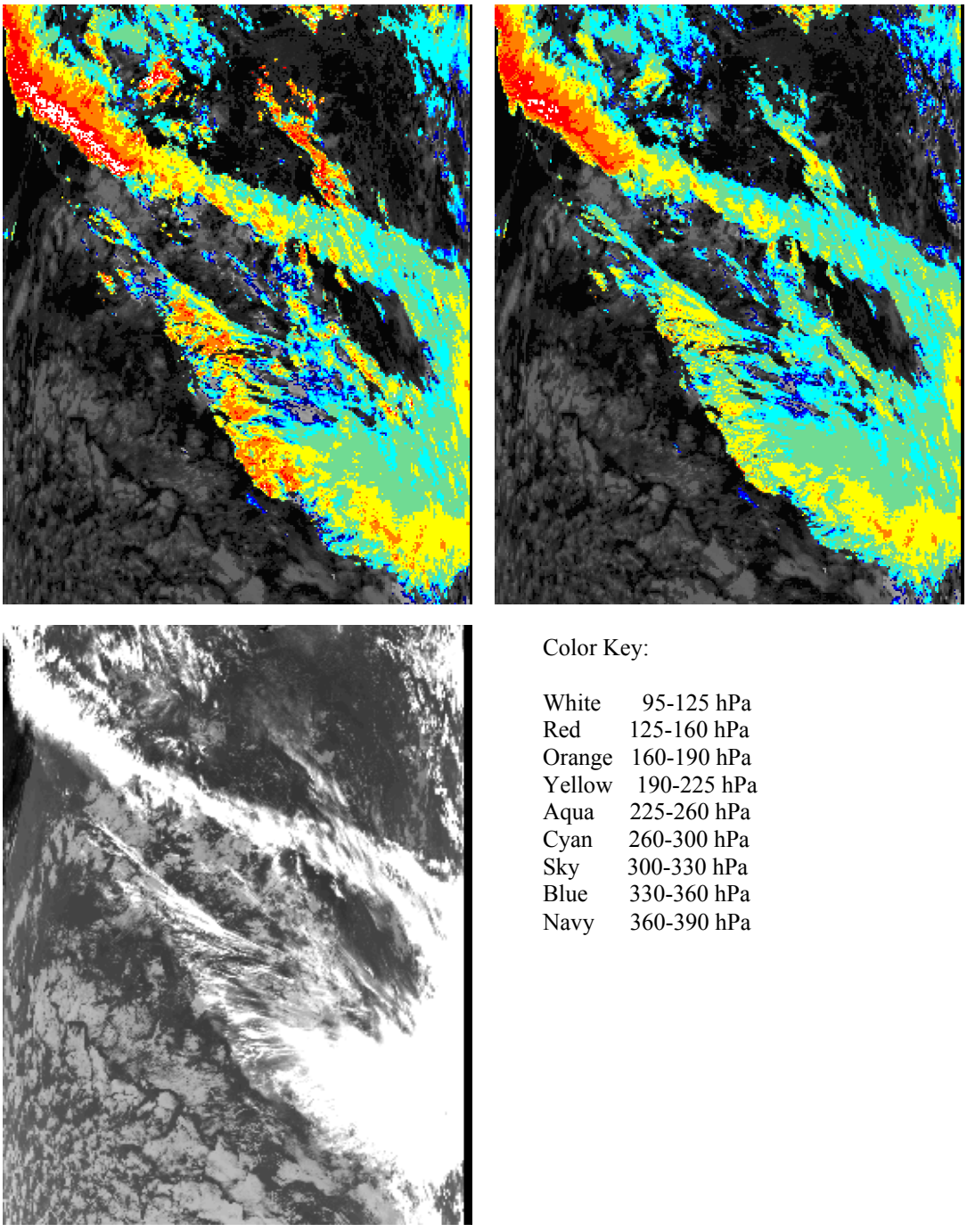

Figure 7. MODIS granule from 1 December 2004 located in the subtropical N. Atlantic. Top left shows cloud top pressures using original method of choosing final cloud top pressure solution (error minimization technique), top right shows new results using "top-down" method. Only high clouds are shown in colors. Bottom left shows band 31 (11.1 μm) brightness temperature image.

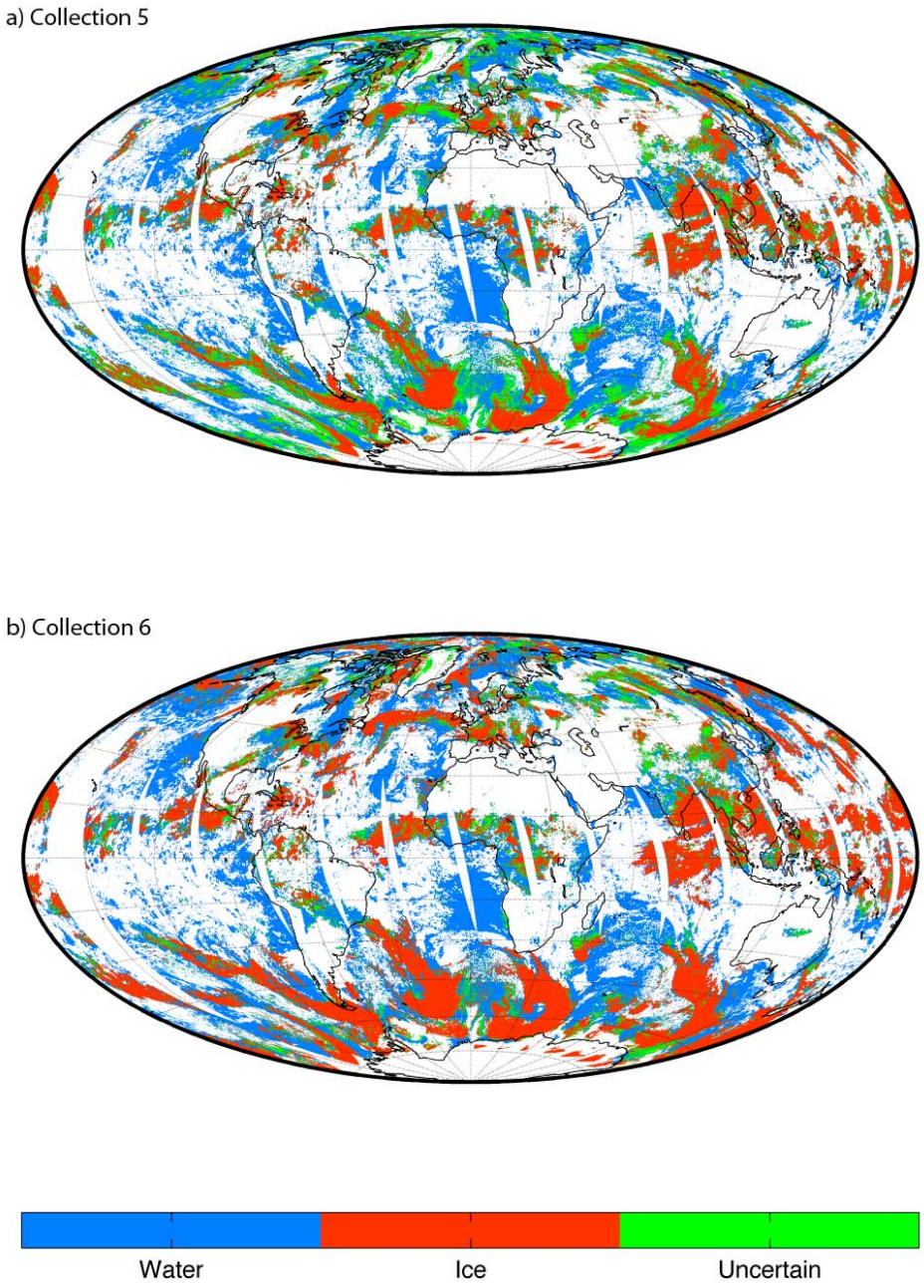

Figure 8: Snap-to-grid daytime results for IR cloud phase on 28 August, 2006, for (a) Collection 5 IR phase algorithm, and (b) new Collection 6 IR cloud phase. For the Collection 5 results, the "mixed-phase" and "undetermined" pixels are merged into the "uncertain" category, as will be done with the Collection 6 1-km and 5-km IR phase product.

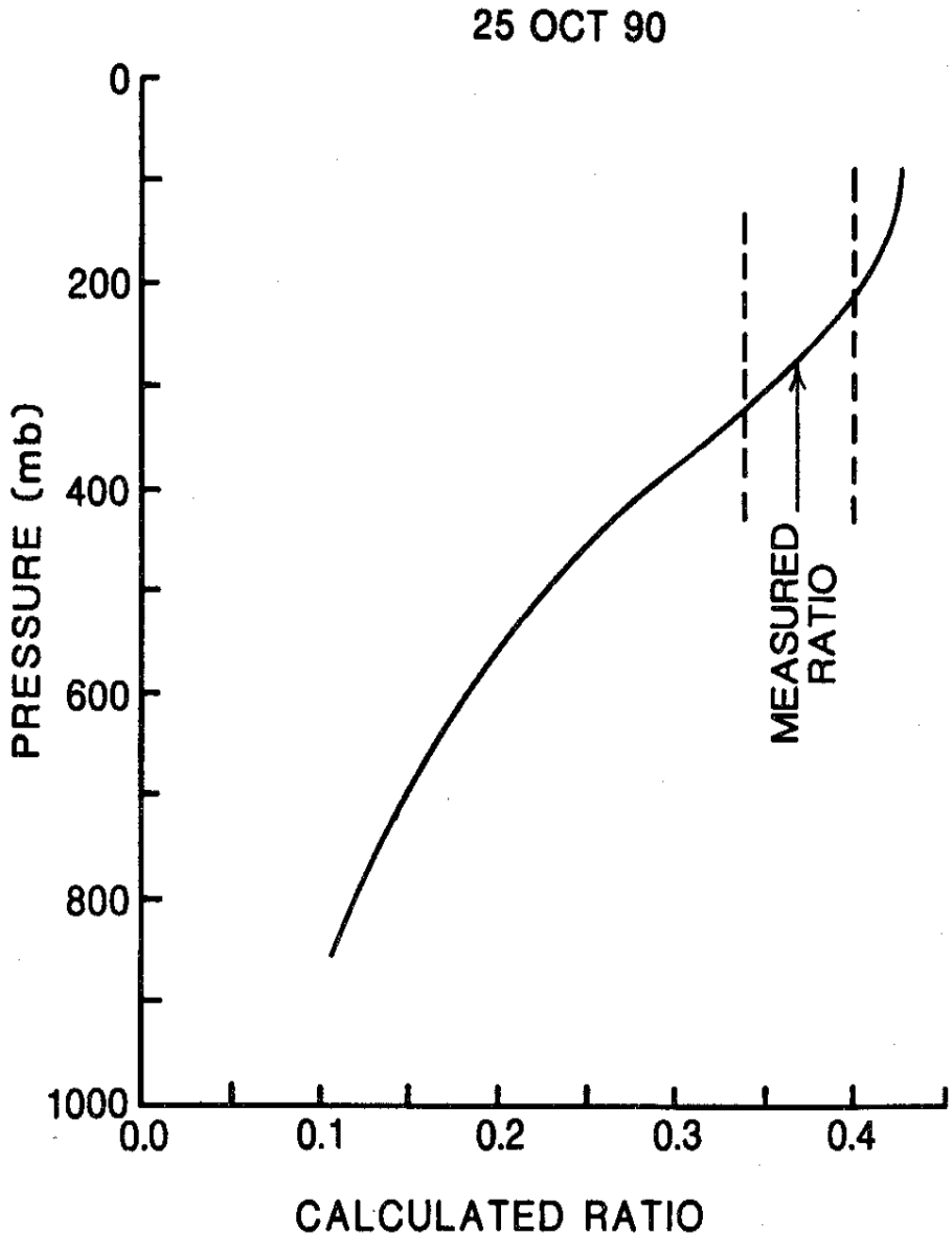

Figure 9. The calculated ratio from the right side of Equation 3 as a function of cloud top pressure from the sounding of 25 October 1990. The measured ratio from the left side of Equation 3 is indicated. The cloud top pressure is inferred to be 300 hPa.

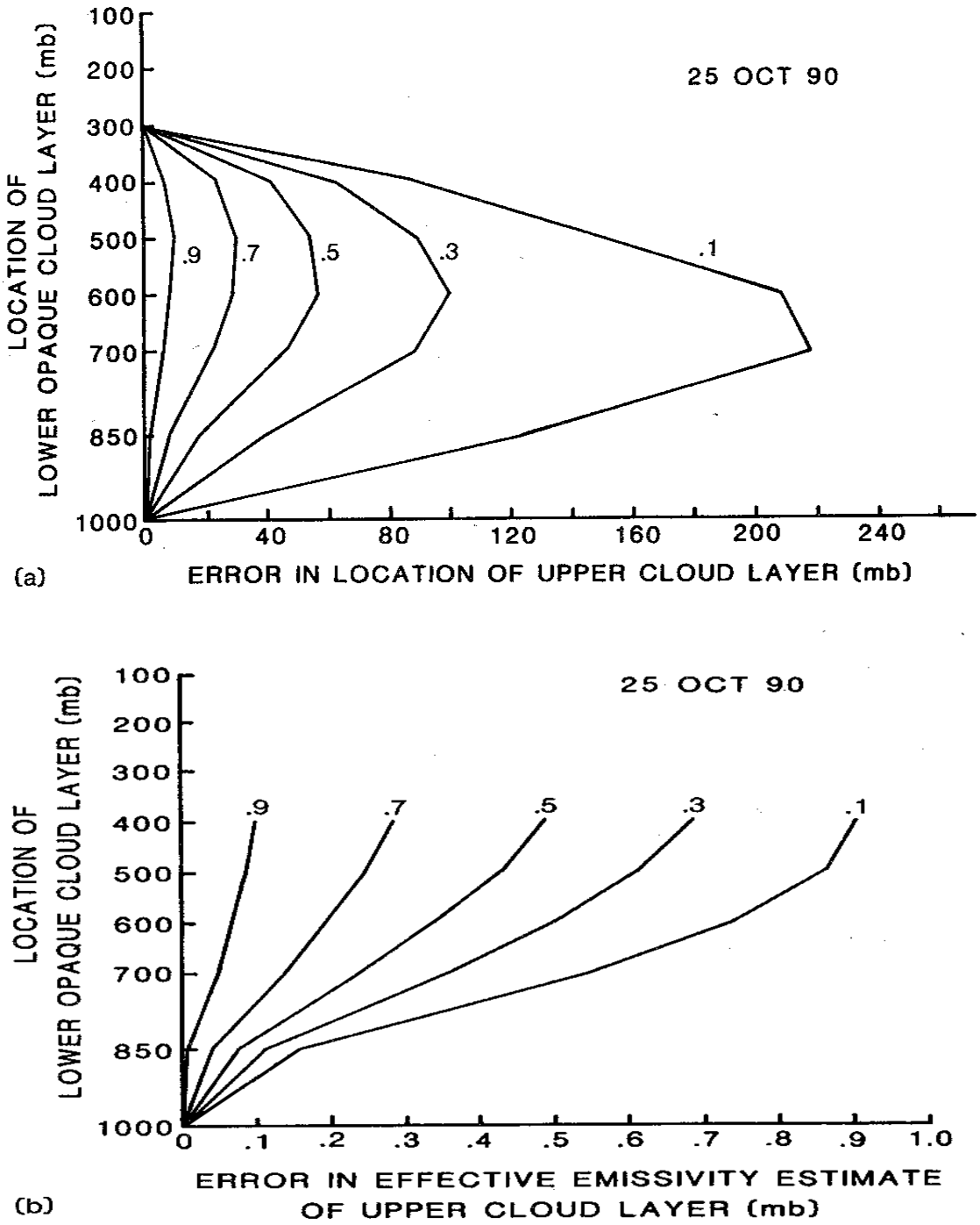

Figure 10. (a) The errors in calculated cloud top pressure (from the original 300 hPa solution) for several different NE as a function of height of the underlying opaque cloud layer. (b) The associated errors in effective emissivity (from the original solution of NE).

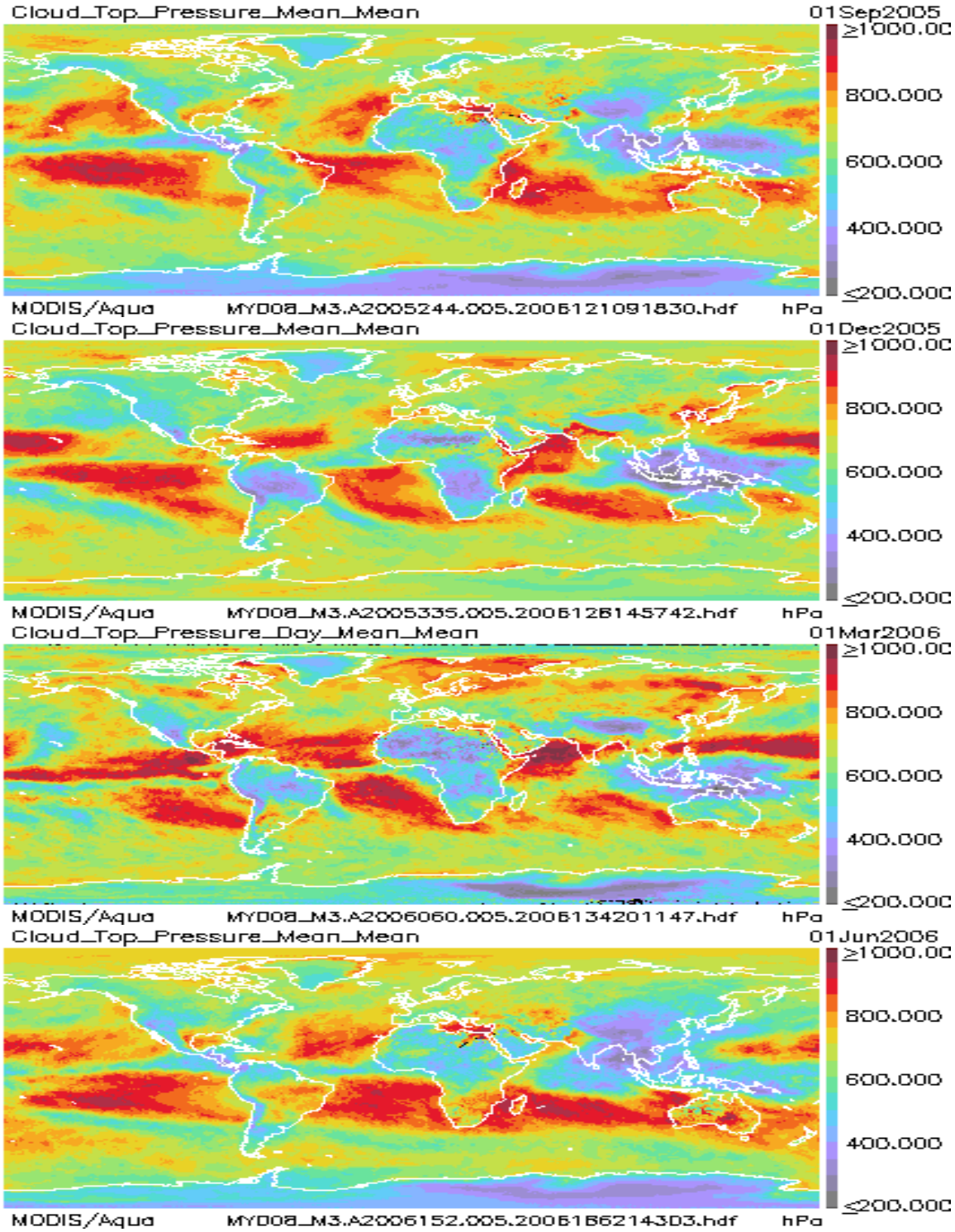

Figure 11: 8-day global distributions of MODIS / Aqua mean cloud top pressures (in hPa compiled for 1 x 1 degree gridded latitude-longitude boxes from the previous eight days) on 1 September 2005, 1 December 2005, 1 March 2006, and 1 June 2006 found at http://modis-atmos.gsfc.nasa.gov/. Red indicates clear sky.

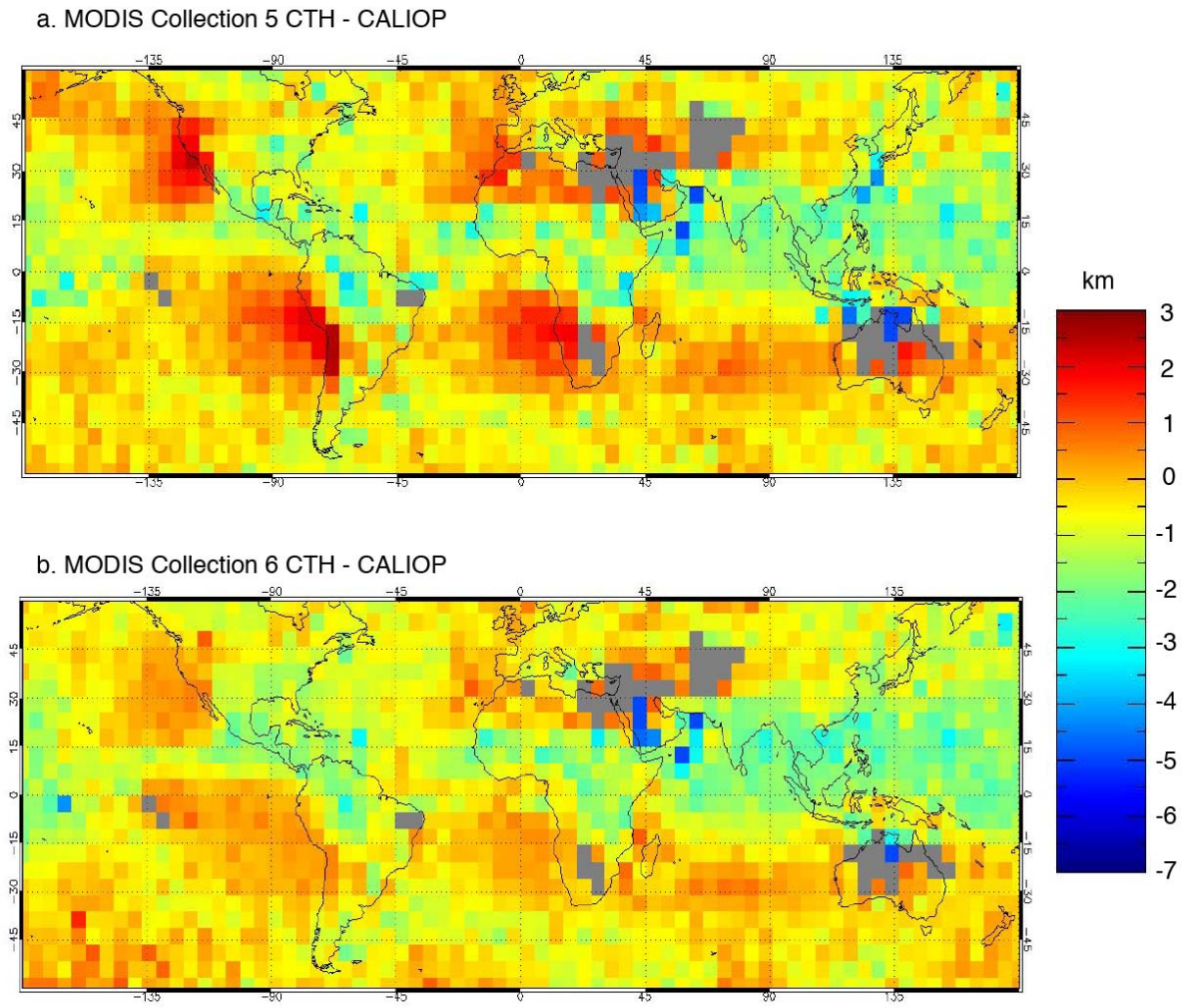

Figure 12: Comparison of mean cloud-top height differences for collocations between MODIS and CALIOP products for August, 2006. The individual collocation CTH differences are averaged in grid cells at 5˚ resolution in latitude and longitude between 60˚N and 60˚S. The results are filtered for single-layered clouds that have an optical thickness ≥ 0.5 as determined from the CALIOP Version 3 product.

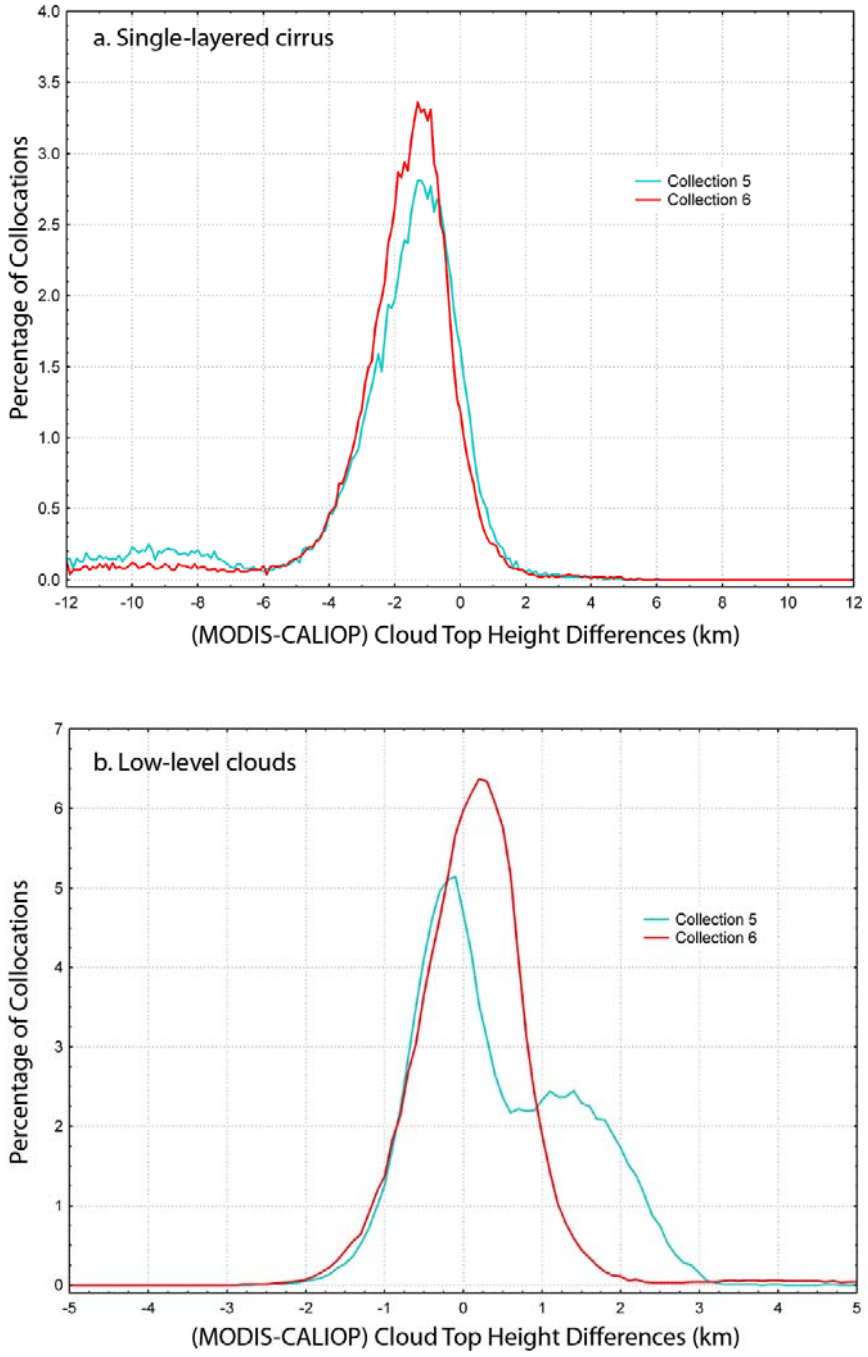

Figure 13: Cloud-top height differences for collocations between MODIS and CALIOP products for August, 2006. The individual MODIS/CALIOP collocations are filtered for (a) single-layered cirrus and (b) low-level clouds. The single-layered cirrus is defined when two conditions are met: (a) CALIOP CTH ≥ 8km and (b) CALIOP sees the surface. A total of 54,992 MODIS–CALIOP collocations met these conditions for single-layered cirrus for August, 2006. Low-level clouds were determined from CALIOP, and there were 259,209 total collocations for the same month. The percentages are calculated at 0.1–km CTH difference resolution.

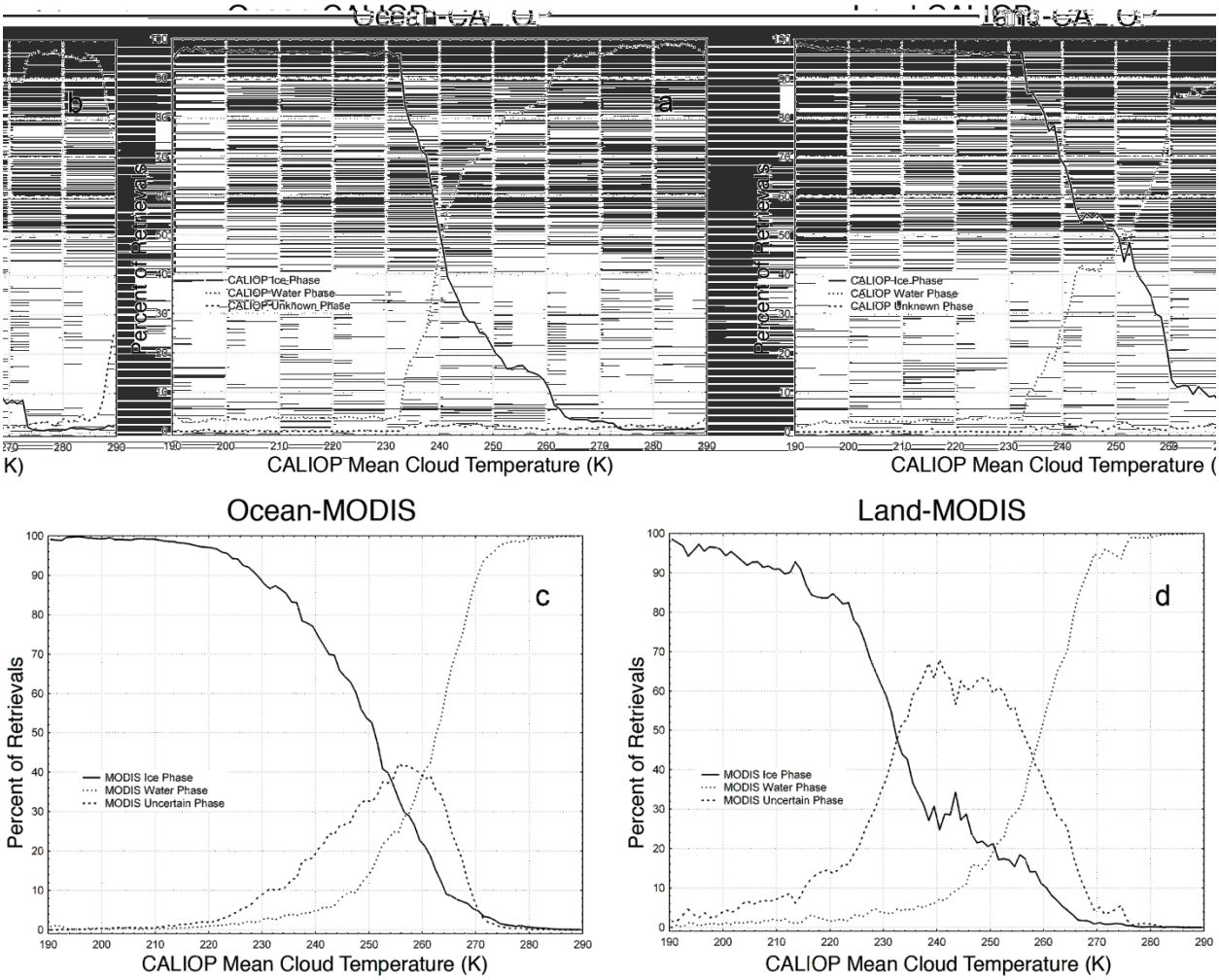

Figure 14: Likelihood of inferring the presence of ice or water cloud as a function of cloud top temperature in the pixel collocations between MODIS and CALIOP for August, 2006. The results are filtered to observations of single-layered clouds that have an optical thickness > 0.5 as determined from the CALIOP Version 3 product. CALIOP cloud phase is presented as a function of CALIOP mean cloud temperature over (a) ocean and (b) land. For comparison, MODIS cloud phase is presented as a function of CALIOP mean cloud temperature over (c) ocean and (d) land. Note that CALIOP has a class called "unknown" in the Version 3 data product while MODIS uses the term "uncertain."

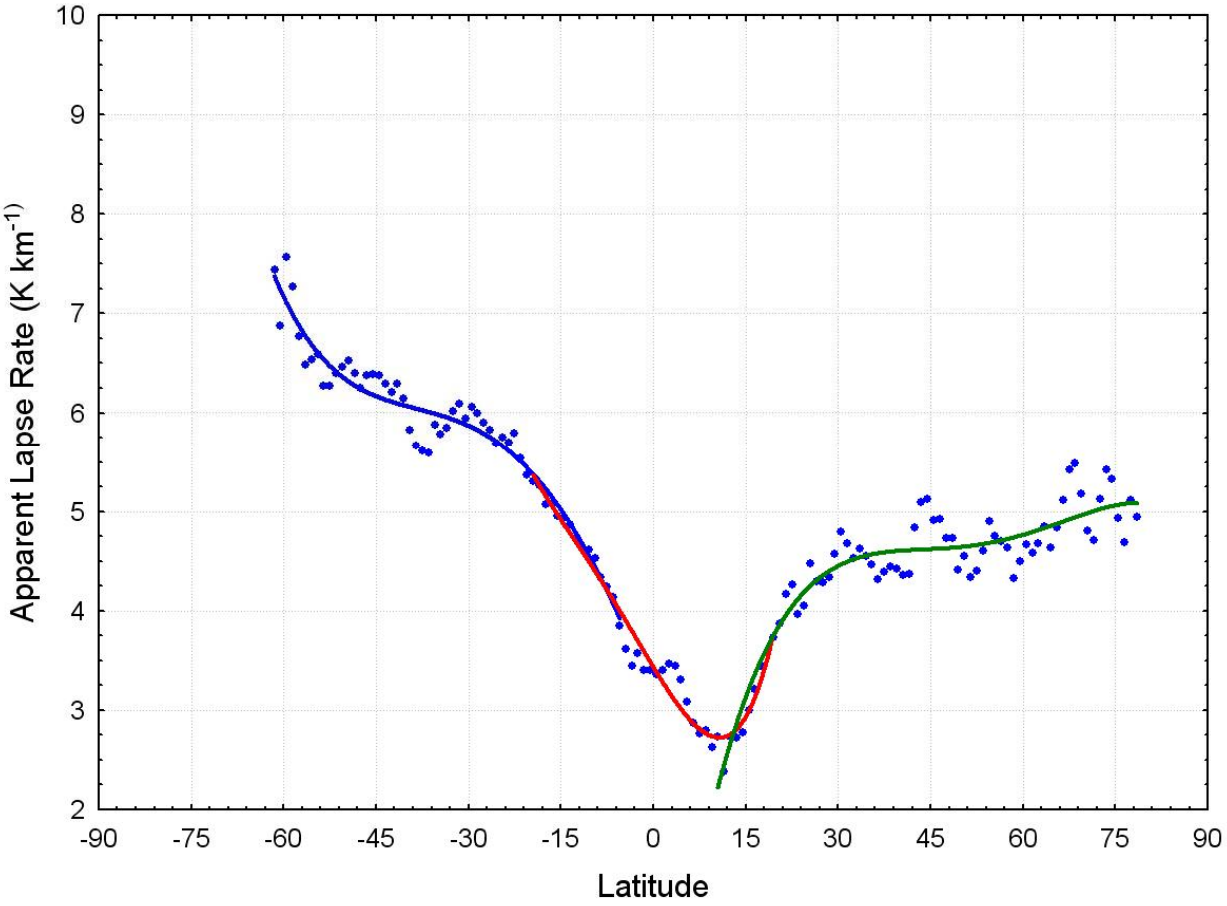

Figure 15: Apparent lapse rates based on 11-μm brightness temperatures as a function of latitude for the month of August. The blue points are the derived zonal mean apparent lapse rates; the blue, red and green lines are polynomial fits to the data. Three separate sets of regression coefficients are calculated: one each for southern and northern hemispheres, and one for the tropics (blue, green, and red lines, respectively). For this month, the "break points" between the three polynomial fits are at 7.8˚S and 19.5˚N latitude.